공학박사학위논문

마찰 계수 및 롤링-슬라이딩 비율을 고려한 트라이포드 타입 등속조인트 축력 예측 모델링

Generated Axial Force Estimation Model of Tripod Type CV Joint Considering Friction Coefficient and Rolling-Sliding Ratio

2017 년 8 월

서울대학교 대학원

기계항공공학부

조 광 희

GENERATED AXIAL FORCE ESTIMATION MODEL OF TRIPOD TYPE CV JOINT CONSIDERING FRICTION COEFFICIENT AND ROLLING-SLIDING RATIO

DISSERTATION

SUBMITTED TO THE SCHOOL OF MECHANICAL

AND AEROSPACE ENGINEEERING AND THE COMMITTEE ON

GRADUATE STUDIES OF SEOUL NATIONAL UNIVERSITY

IN PARTIAL FULFILLMENT OF THE REQUIREMENTS

FOR THE DEGREE OF DOCTOR OF PHILOSOPHY

Gwang Hee Jo

August 2017

Abstract

Gwang Hee Jo

School of Mechanical and Aerospace Engineering

The Graduated School

Seoul National University

This study proposes a new Generated Axial Force (GAF) estimation model of tripod type Constant Velocity (CV) joints. In order to overcome weakness of the existing methods which didn't consider or simplified friction characteristics, this study consider the rolling-sliding ratio and the friction coefficient based on the experimental analysis.

In the first step of the development of the model, kinematic analysis was performed to derive the relative coordinates of components and contact points. Through the analysis, the normal load that acts on contact points was also obtained. This study employs two friction characteristics – pure sliding friction

characteristics and rolling-sliding friction characteristics – to obtain the friction coefficients on the contact points. Especially for rolling-sliding friction, this study used the experimental analysis on rolling-sliding ratio and then, friction coefficients were also studied by using a tribometer. By introducing two friction characteristics, this study considers not only the pure sliding friction but also the rolling-sliding friction that occurs between spherical rollers and tracks.

This study verifies the GAF estimation model by comparing the simulation results with the experimental results. A tripod type CV joint was set as a target and its GAF was derived by the model. Then, its actual GAF was measured and the results were compared with each other. For the measurement, a GAF measurement system was set up in this study. The estimated results shows the similar tendency with the measured results at low resistance torque condition and furthermore, the GAF model provides very accurate estimation at high resistance torque conditions.

By using the developed GAF model, GAF factors were analyzed. The influence of the GAF factors on the GAF was analyzed and then the influence on the GAF factors was verified through a GAF measurement system. New prototypes with the changed design parameters were manufactured and its GAF were measured. Based on the results, the optimized design parameters were selected and its GAF was also verified. As a final outcome of this study, GAF reduction was achieved.

Keywords: Generated Axial Force, GAF, Constant Velocity joint, CV joint, Tripod type CV joint, normal load, relative coordinate, friction characteristics, friction coefficient, rolling-sliding ratio, RSR, spherical roller, track, track curvature, contact angle, normal pressure, velocity, GAF reduction

Student number: 2010-23233

Contents

List of Figures

List of Tables

Chapter 1

1. Introduction

1.1 Research background

Drive shafts transmit power from a transmission to wheels. When a vehicle goes on a bumpy road, the drive shafts still have to transmit power through a variable angle at constant rotational speed and accordingly, they need CV joints. CV joints are located at the both ends of drive shafts – Inner CV joints connect the drive shafts to the transmission, while outer CV joints connect the drive shafts to the wheels as shown in Figure 1.1. Inner CV joints which are called inboard joints have angular and axial displacement. They act as a damper when a plunging motion is applied to the drive shaft so that the length of the drive shaft can be changed. Outer CV joints which are called outboard joints have large articulation angle so that they enable the wheels to steer. Generally, tripod type joints are used

as inboard joints and ball type joints are used as outboard joints [1].

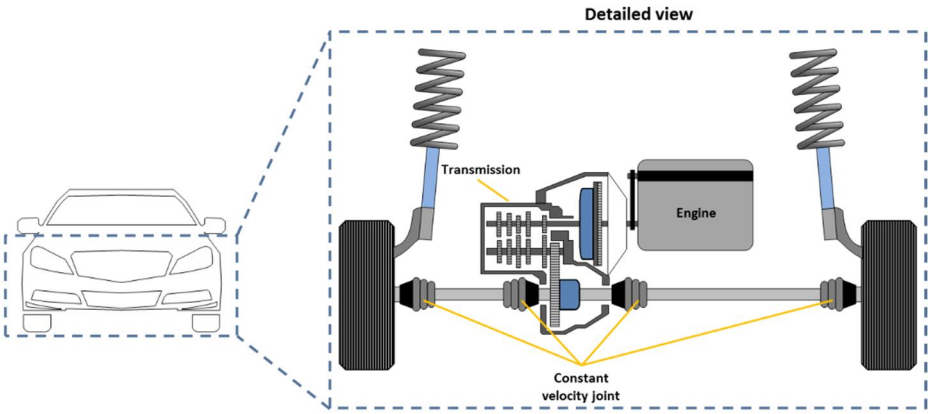

Figure 1.1 Constant velocity joint

Tripod type CV joints consist of three spherical rollers. The rollers have 120 degrees phase difference each other and each roller has one spherical roller, multiple needle rollers and trunnions. Ball type CV joints, on the other hand, consists of outer race, cage, balls and inner race. The number of balls used in ball type CV joints is 6 or 8 in general [2].

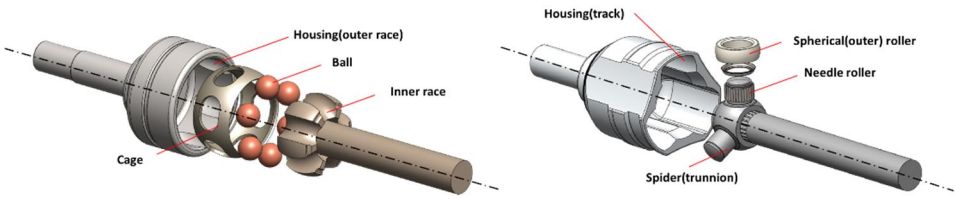

(a) **(b)**

Figure 1.2 Types of constant velocity joint (a) ball type constant velocity joint and (b) tripod type constant velocity joint

There are mainly three issues regarding CV joints – shudder effect, idle booming and efficiency loss [1]. Shudder effect is caused by GAF. When a vehicle is accelerated abruptly, high torque is applied on the CV joints. Then, the torque generates mechanical friction between the track and the spherical roller. Through this process, GAF is cause by the friction and it is transmitted to the vehicle and it becomes lateral force of the vehicle. The lateral force causes vehicle vibration and bad ride comfort.

Idle booming is caused by Plunging Force (PF) when a vehicle is in idle state.

Engine vibration is transmitted to the CV joints and it generates plunging motion of the CV joints. The plunging motion generates axial force by the mechanical friction and .the axial force is called PF. The PF is transmitted to the vehicle frame and it causes structure resonance. It causes vehicle vibration and bad ride comfort. These GAF and PF are caused by the internal friction of CV joints but GAF is caused by reciprocation motion between spherical rollers and tracks when the vehicle is accelerated, while PF is occurred by the plunging motion of inboard joints when the vehicle is stationary.

Efficiency loss is caused by the internal friction between components. It results in the increase of temperature and the loss of fuel efficiency.

Among these issues, the shudder effect is the most problematic. It is becoming the most serious problem of CV joint and it gives a driver bad ride comfort. In order to solve this problem, a reliable GAF estimation model is needed.

In this study, in order for the development of a new GAF model, a kinematic

analysis was performed to find the relative coordinates and the contact points of each component and then, integrated friction characteristics were analyzed, which included pure sliding friction and rolling-sliding friction. In this part, the friction characteristics between the components were researched in detail by analyzing pure sliding motion and rolling-sliding motion and the friction coefficients between the contact points were measured under actual driving conditions via a tribometer. In addition, the rolling-sliding ratio between spherical rollers and tracks was also analyzed. A new GAF model employed this friction characteristics in order to estimate the GAF values of a tripod type CV joint and the estimation results were verified by experimental results. In order for the verification, a GAF measurement system was set up and a tripod type CV joint was designated as a target. Finally, the GAF model was experimented by applying its actual driving conditions into the model and the GAF measurement system.

By using the development GAF model, GAF factor analysis was carried out and based on the results, direction for GAF reduction was suggested and it was

verified through a GAF measurement system.

1.2 Previous research

In order to solve issues related to CV joints, many researchers have studied tripod type CV joints. Watanabe et al. analyzed relative motion of rollers and tracks through kinematic and static analyses [3] and a numerical model of ball and tripod type CV joints was developed through dynamic analyses by Lim et al. [4]. Serveto et al. developed a GAF model considering internal friction from two models: Coulomb model and Adams model [5, 6]. Lee and Polycarpou studied friction models of tripod type CV joints to estimate GAF [7]. Urbinati and Pennestri performed kinematic analysis on tripod type CV joints [8]. Mariot and K'Nevez performed kinematics of tripod type CV joint analyzed based on the threefold symmetry of the tripod type CV joint [9] and by using the results, they also performed kinematics on the ball type CV joint and integrated them with the

tripod type CV joint [10]. They also studied dynamics of CV joints and developed a kinetostatic model including friction [11, 12]. Wang and Chang el al. performed kinematic analysis on tripod type CV joints [13] and considered their lubricant properties [14, 15]. Numeric analysis and experiments approaches were also studied by Kimata et al. [16]

Despite all studies on tripod type CV joints, only pure sliding motion has been considered as relative motion. The actual rolling-sliding motion between rollers and tracks has not been considered in most studies. In most studies, friction characteristics were not considered or they were simplified. It can lower the reliability of the studies.

In this study, therefore, a new GAF model of tripod type CV joints was developed, which considers not only pure sliding motion but also rolling-sliding motion.

1.3 Research objective

This study proposes a theoretical modeling method of the GAF and its reduction. The first objective, the theoretical modeling and its verification, is the accurate modeling of the GAF estimation. In order to predict the GAF of the tripod CV joint, the kinematic analysis was performed, the detailed friction characteristics were analyzed, the rolling-sliding ratios were analyzed experimentally and the GAF estimation of the tripod CV joint was modeled and verified.

The second objective, reduction of the GAF problem, is to propose a solution of GAF problem. In order to suggest the solution, the GAF estimation model was employed. By using the model, the parameters related with the GAF was analyzed and the optimal design parameters were suggested. The GAF of new prototypes which have the optimal design parameters was measured and the reduction of the GAF was achieved.

This study proposes a theoretical modeling method of GAF to analyze and reduce the GAF. The proposed method can be solutions for the problems of the existing method.

- The GAF estimation model employs in this study can provide accurate prediction of the GAF. The model includes the detailed friction characteristics which consists of rolling-sliding friction and pure sliding friction. Most papers didn't consider the rolling-sliding friction model and are less accurate. In this study, friction characteristics were studied in detail through experimental analysis of friction coefficient and rolling-sliding ratio.

- The proposed method enables CV joint manufacturers to cope with change of CV joint's specifications. CV joints vary from vehicle to vehicle and require design optimization depending on size and performance of vehicle. Size of CV joint is selected according to

vehicle performance and space constraints. Based on the selected size, GAF characteristics according to driving conditions are analyzed through this model. Based on the analyzed GAF characteristics, the GAF reduction can be achieved by optimizing the design parameters. That is, time and cost savings are possible by optimizing design parameters in the design process before measuring the actual GAF characteristics.

- In addition, the proposed model can be used for idle booming and efficiency loss analysis. Since the idle booming and the efficiency loss are also caused by the mechanical friction inside the CV joint, the results of the friction characteristics of this study can be applied and analyzed. In other words, by using this model, it is possible to analyze not only bad ride problem related to CV joint but also performance of CV joint.

1.4 Dissertation overview

The remainder of this dissertation is organized as follows:

Chapter 2 : GAF estimation modeling presents a method to model GAF of CV joint. First step of development of GAF estimation model, a kinematic analysis was performed and as a result, relative coordinates of the components and contact points were derived. Based on the kinematic analysis, normal force of each contact point was calculated from driving conditions. In order to develop a reliable GAF estimation model, an integrated friction characteristics were analyzed. A pure sliding friction characteristics and rolling-sliding friction characteristics were integrated. In the pure sliding friction characteristics, analysis on the pure sliding friction coefficient was carried out. In the rolling-sliding friction characteristics, rolling-sliding ratio was analyzed through experimentally by using a rolling-sliding ratio measurement system. To analyze friction characteristics in detail, a tribometer and a rolling-sliding ratio measurement system were set up to measure friction coefficient and rolling-sliding ratio

respectively. After analysis on the friction characteristics, they were applied to the GAF estimation model.

Chapter 3 : GAF reduction using GAF estimation model presents a method to reduce GAF of target CV joint. In this chapter, analysis of GAF factors was performed. The factors directly related to the GAF are friction coefficient, rolling-sliding ratio and normal load. The normal load is related to the driving conditions. Thus, the GAF reduction was analyzed by approaching the friction coefficient and rolling-sliding ratio. The factors are commonly associated with the friction coefficient and the rolling-sliding ratio are related with normal pressure and velocity. Then, final step of the factor analysis, design parameters related to the normal pressure and velocity were analyzed. Based on the results, GAF was estimated according to the change of the design parameters and new prototypes which have changed design parameters were manufactured and its GAF was

measured through GAF measurement system. After that, direction for GAF reduction was suggested and its verification was performed by comparing the measured GAF and estimated GAF. As a final outcome, GAF reduction was achieved.

Chapter 4 : Conclusion provides a summary of the study.

Chapter 2

2. GAF estimation model

2.1. Kinematic analysis

As the first step for GAF estimation in this study, the relative coordinates of each component were derived through kinematic analysis.

In tripod type CV joints, three spherical rollers have 120 degrees of phase difference each other. They move along the tracks as the CV joint rotates and they have two relative motions to the tracks – pure sliding motion and rolling-sliding motion. In order to establish a GAF model, the relative motions of each part and the contact points need to be obtained.

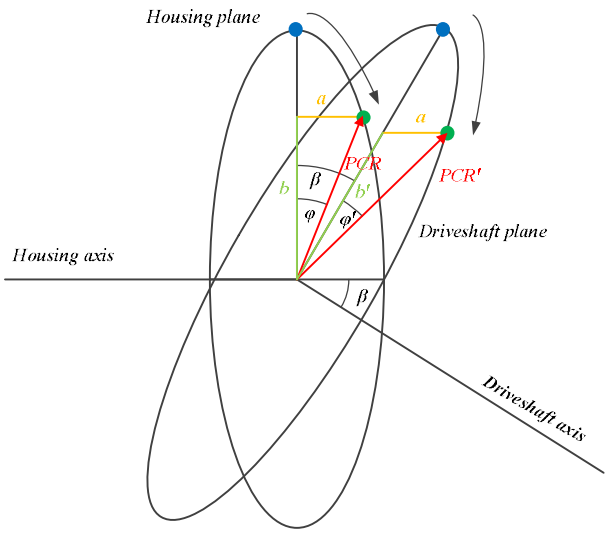

Figure 2.1 Change of phase angle and PCR under articulated condition

The coordinate system of CV joint housing can be transformed to the roller center coordinate system by the following equation.

$$\begin{pmatrix} x \\ y \\ z \end{pmatrix}_{Roller\ center} = \begin{pmatrix} \cos(-\beta) & \sin(-\beta) & 0 \\ -\sin(-\beta) & \cos(-\beta) & 0 \\ 0 & 0 & 1 \end{pmatrix}^{-1} \begin{pmatrix} 1 & 0 & 0 \\ 0 & \cos\varphi' & \sin\varphi' \\ 0 & -\sin\varphi' & \cos\varphi' \end{pmatrix}^{-1} \begin{pmatrix} 0 \\ PCR' \\ 0 \end{pmatrix} \quad (2.1)$$

where φ = phase angle in housing plane, φ' = phase angle in driveshaft plane, β = articulation angle, PCR = pitch circle radius in housing plane, PCR' = pitch circle radius in driveshaft plane as shown in Figure. 2.1.

In equation (2.1), articulation angle and phase angle are considered. The center coordinate of a spherical roller pair can be represented by the following equation.

$$\begin{pmatrix} x \\ y \\ z \end{pmatrix}_{Roller\ center} = \begin{pmatrix} PCR' \cos\varphi' \sin\beta \\ PCR' \cos\varphi' \cos\beta \\ PCR' \sin\varphi' \end{pmatrix} \quad (2.2)$$

Here, φ' which is phase angle in driveshaft plane can be obtained from phase angle in housing plane, φ.

In Figure 2.1, φ' is obtained from a, b and b', which are virtual variables. φ' can be obtained by the following equations.

$$a = PCR \sin \varphi \tag{2.3}$$

$$b = PCR \cos \varphi = b' \cos \beta \tag{2.4}$$

$$\tan \varphi' = \frac{a}{b'} = \frac{PCR \sin \varphi}{\frac{b}{\cos \beta}} = \frac{\sin \varphi \cos \beta}{\cos \varphi} = \tan \varphi \cos \beta \tag{2.5}$$

$$\varphi' = \tan^{-1}(\tan \varphi \cos \beta) + \psi \tag{2.6}$$

where $\psi = 0, \pi$ and 2π, which varies with phase angle.

PCR' is formed by the relative motion between a spherical roller and a needle roller in the direction of the trunnion axis and its trajectory is an elliptical shape as shown in Figure 2.1. It varies with phase angle and can be obtained by the following equation.

$$PCR' = \frac{PCR^2}{\cos\beta \sqrt{(PCR\cos\varphi')^2 + \left(\frac{PCR}{\cos\beta}\sin\varphi'\right)^2}} \quad (2.7)$$

From equations (2.2), (2.6) and (2.7), the center coordinate of a spherical roller pair is

$$\begin{pmatrix} x \\ y \\ z \end{pmatrix}_{Roller\ center} = \begin{pmatrix} \dfrac{PCR^2 \tan\beta \cos(\tan^{-1}(\tan\varphi\cos\beta)+\psi)}{\sqrt{(PCR\cos(\tan^{-1}(\tan\varphi\cos\beta)+\psi))^2 + \left(\frac{PCR}{\cos\beta}\sin(\tan^{-1}(\tan\varphi\cos\beta)+\psi)\right)^2}} \\ \dfrac{PCR^2 \cos(\tan^{-1}(\tan\varphi\cos\beta)+\psi)}{\sqrt{(PCR\cos(\tan^{-1}(\tan\varphi\cos\beta)+\psi))^2 + \left(\frac{PCR}{\cos\beta}\sin(\tan^{-1}(\tan\varphi\cos\beta)+\psi)\right)^2}} \\ \dfrac{PCR^2 \sin(\tan^{-1}(\tan\varphi\cos\beta)+\psi)}{\cos\beta\sqrt{(PCR\cos(\tan^{-1}(\tan\varphi\cos\beta)+\psi))^2 + \left(\frac{PCR}{\cos\beta}\sin(\tan^{-1}(\tan\varphi\cos\beta)+\psi)\right)^2}} \end{pmatrix} \quad (2.8)$$

The coordinate of the contact point between a trunnion and a needle roller can be also obtained in the same way. It is represented by the following equation.

$$\begin{pmatrix} x \\ y \\ z \end{pmatrix}_{Trunnion-needle} = \begin{pmatrix} \frac{PCR^2 \tan\beta \cos(\tan^{-1}(\tan\varphi \cos\beta) + \psi)}{\sqrt{(PCR\cos(\tan^{-1}(\tan\varphi\cos\beta)+\psi))^2 + \left(\frac{PCR}{\cos\beta}\sin(\tan^{-1}(\tan\varphi\cos\beta)+\psi)\right)^2}} \\ (PCR - r_t)\cos\varphi \\ (PCR - r_t)\sin\varphi \end{pmatrix} \quad (2.9)$$

where r_t = radius of trunnion.

The coordinate of the contact point between a needle roller and a spherical roller can be also obtained in the same way. It is represented by the following equation.

$$\begin{pmatrix} x \\ y \\ z \end{pmatrix}_{Needle-spherical} = \begin{pmatrix} \frac{PCR^2 \tan\beta \cos(\tan^{-1}(\tan\varphi \cos\beta) + \psi)}{\sqrt{(PCR\cos(\tan^{-1}(\tan\varphi\cos\beta)+\psi))^2 + \left(\frac{PCR}{\cos\beta}\sin(\tan^{-1}(\tan\varphi\cos\beta)+\psi)\right)^2}} \\ (PCR - r_t - r_n)\cos\varphi \\ (PCR - r_t - r_n)\sin\varphi \end{pmatrix} \quad (2.10)$$

where r_n = radius of needle roller.

When a tripod type CV joint has two-point contacts between the spherical roller and the track as shown in Figure 2.2 (a), the contact points form yaw angles as the phase angle changes as shown in Figure 2.2 (b).

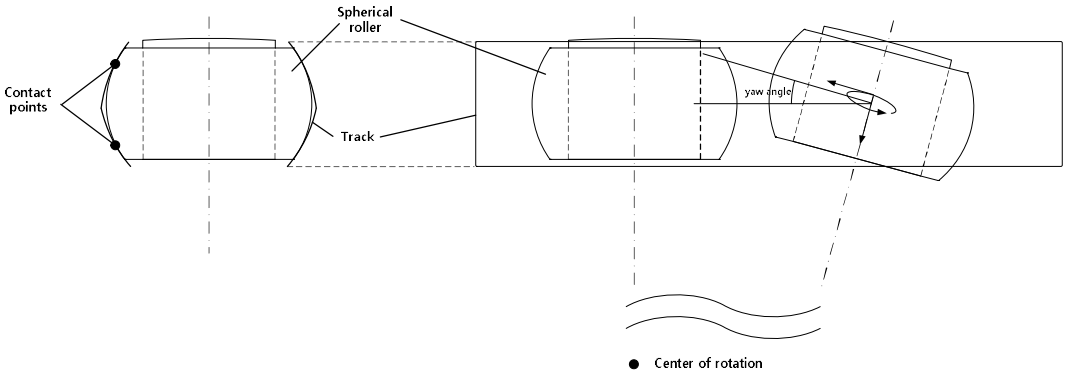

Figure 2.2 Spherical roller and track in (a) front view (b) side view

The yaw angle between a spherical roller and a track is obtained by the

following equation:

$$\alpha = \cos^{-1}\frac{PCR}{PCR'} \tag{2.11}$$

$$= \cos^{-1}\left(\cos\beta\sqrt{(\cos(\tan^{-1}(\tan\varphi\cos\beta)+\psi))^2+\left(\frac{\sin(\tan^{-1}(\tan\varphi\cos\beta)+\psi)}{\cos\beta}\right)^2}\right)$$

where α = yaw angle.

There are four contact points in one spherical roller and track pair, two occurs in one side of the track and the other two in the other side. The contact points can be obtained by the following equations, respectively.

$$\begin{pmatrix}x\\y\\z\end{pmatrix}_{Spherical-track,upper} = \tag{2.12}$$

$$\begin{pmatrix}\dfrac{PCR^2\tan\beta\cos(\tan^{-1}(\tan\varphi\cos\beta)+\psi)}{\sqrt{\left(PCR\cos(\tan^{-1}(\tan\varphi\cos\beta)+\psi)\right)^2+\left(\dfrac{PCR}{\cos\beta}\sin(\tan^{-1}(\tan\varphi\cos\beta)+\psi)\right)^2}}\\ PCR\cos\varphi + r_s\cos\delta\sin\varphi + r_s\sin\delta\cos\varphi\\ PCR\sin\varphi - r_s\cos\delta\cos\varphi + r_s\sin\delta\sin\varphi\end{pmatrix}$$

$$\begin{pmatrix} x \\ y \\ z \end{pmatrix}_{Spherical-track,lower} = \begin{pmatrix} \frac{PCR^2 \tan\beta \cos(\tan^{-1}(\tan\varphi \cos\beta) + \psi)}{\sqrt{(PCR\cos(\tan^{-1}(\tan\varphi\cos\beta)+\psi))^2 + \left(\frac{PCR}{\cos\beta}\sin(\tan^{-1}(\tan\varphi\cos\beta)+\psi)\right)^2}} \\ PCR\cos\varphi + r_s\cos\delta\sin\varphi - r_s\sin\delta\cos\varphi \\ PCR\sin\varphi - r_s\cos\delta\cos\varphi - r_s\sin\delta\sin\varphi \end{pmatrix} \quad (2.13)$$

where r_s = radius of spherical roller, δ = contact angle between spherical roller and track.

TABLE 2.1 Driving conditions of CV joint

Resistance torque (Nm)	100, 200, 300, 400
Rotation speed (rpm)	50, 100, 150, 200
Articulation angle (deg)	0, 3, 6, 9, 12

The relative coordinates of components and contact points are affected by the driving conditions such as rotation speed and articulation angle. The conditions of simulation are the same as the driving conditions given in TABLE 2.1. In the simulation, the maximum rotation speed and articulation angle were used to clarify the differences between the relative coordinates.

The coordinates of roller centers are shown in Figure 2.3.

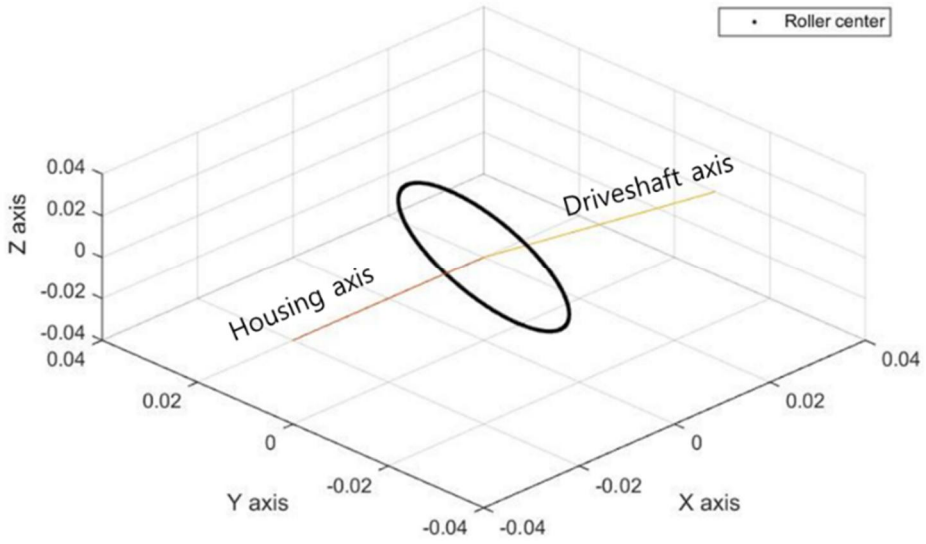

Figure 2.3 Coordinate of roller center

The coordinates of contact points are shown in Figure 2.4.

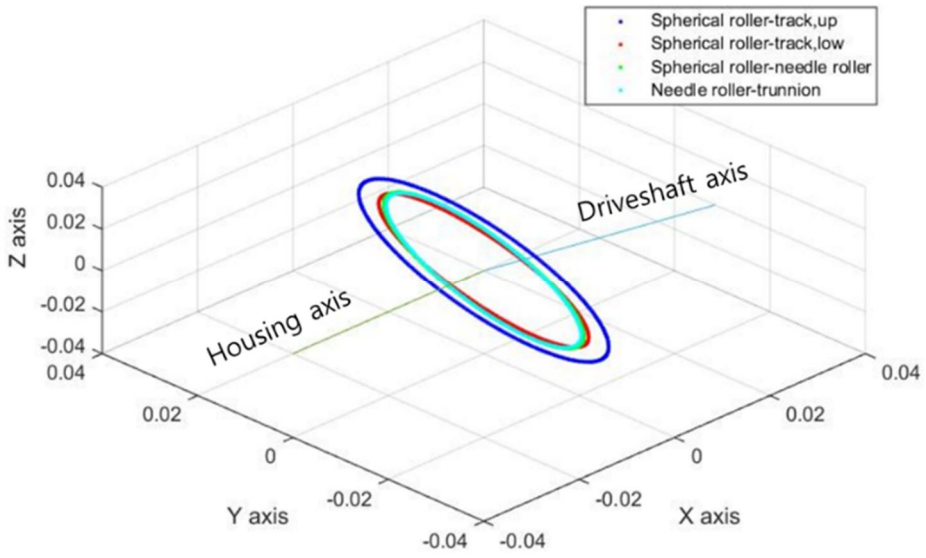

Figure 2.4 Coordinate of contact points

By using equation (2.7) and (2.11), PCR' and yaw angle were derived. Figure 2.5 shows PCR' according to phase angle and Figure 2.6 shows yaw angle according to phase angle in 12 degrees of articulation angle. As phase angle goes,

PCR' fluctuates with 180 degrees cycle whereas yaw angle fluctuates with 360 degrees cycle. Especially for yaw angle, it has both of positive and negative values and therefore, it determines the sign of GAF.

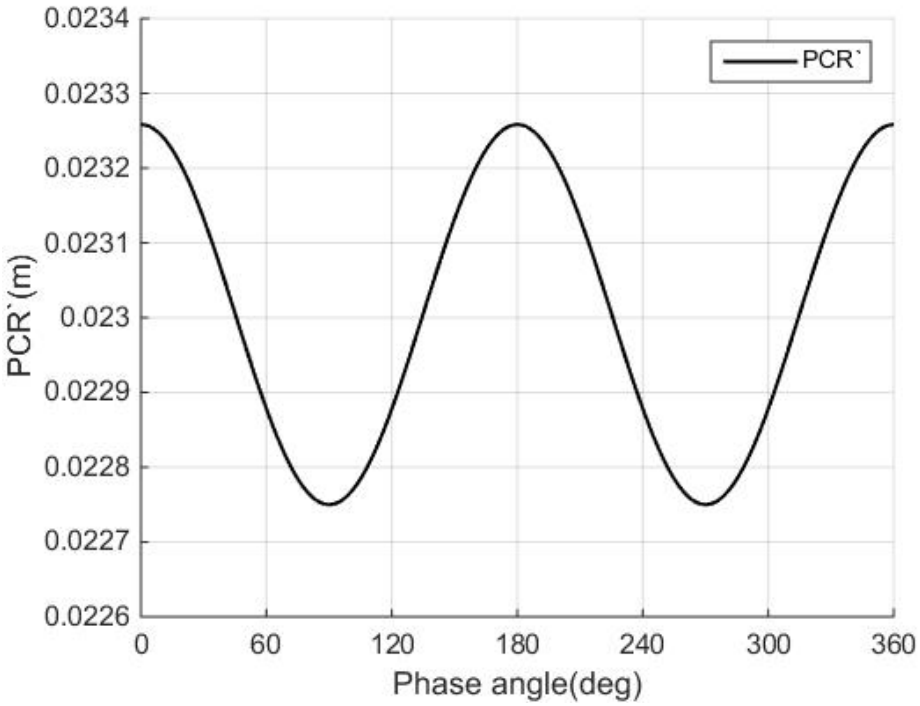

Figure 2.5 PCR' according to phase angle

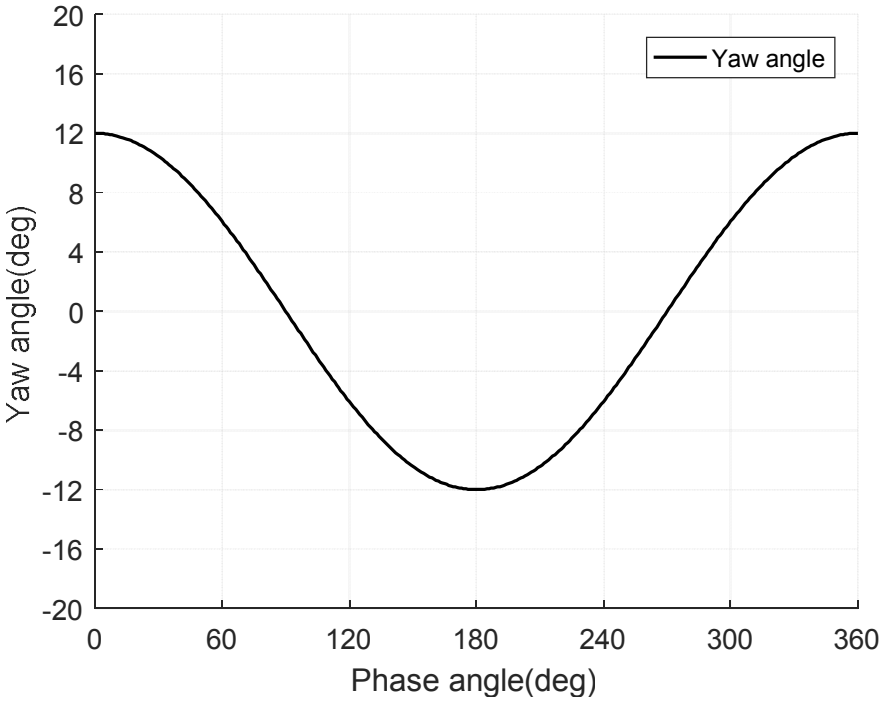

Figure 2.6 Yaw angle according to phase angle

2.2. Normal force derivation

When torque is applied on a CV joint, normal load occurs at the contact points. Normal load can be calculated from the driving conditions of the CV joint and the relative motion obtained in the previous chapter. Normal load can be obtained by the following equations:

$$N_1 r_1 + N_2 r_2 + N_2 r_2 = T \quad (2.14)$$

$$\overrightarrow{N_1} + \overrightarrow{N_2} + \overrightarrow{N_3} = 0 \quad (2.15)$$

where N_1, N_2, N_3 = normal load between spherical roller and track, r_1, r_2, r_3 = moment arms from the center of the joints to center of spherical rollers,

r_1, r_2, r_3 are obtained from equation (2.8) – (2.13).

$$r_t = \sqrt{\left(\frac{PCR^2\cos(\tan^{-1}(\tan\varphi\cos\beta)+\psi)}{\sqrt{(PCR\cos(\tan^{-1}(\tan\varphi\cos\beta)+\psi))^2+\left(\frac{PCR}{\cos\beta}\sin(\tan^{-1}(\tan\varphi\cos\beta)+\psi)\right)^2}}\right)^2 + \left(\frac{PCR^2\sin(\tan^{-1}(\tan\varphi\cos\beta)+\psi)}{\cos\beta\sqrt{(PCR\cos(\tan^{-1}(\tan\varphi\cos\beta)+\psi))^2+\left(\frac{PCR}{\cos\beta}\sin(\tan^{-1}(\tan\varphi\cos\beta)+\psi)\right)^2}}\right)^2} \quad (2.16)$$

Considering the geometry of CV joints, it is assumed that each normal load that acts on the contact points of spherical rollers and tracks has the same magnitude and they are proportional to the torque applied to the driveshaft [3].

2.3. Friction characteristics analysis

In tripod type CV joints, GAF is created by the internal friction between the components. The main factor of GAF is the friction between spherical rollers and tracks [11]. When a tripod type CV joint rotates, the spherical rollers and the

tracks form yaw angles as shown in Figure 2.1. The yaw angle varies in the range from the negative articulation angle to the positive articulation angle.

As spherical rollers moves along the tracks, not only rolling-sliding motion but also pure sliding motion occur between the rollers and the tracks [17-20]. In the direction of the trunnion axis, only sliding motion occurs because the axis is perpendicular to the rolling direction. In the radial direction of the rollers, on the other hand, rolling-sliding mixed motion occurs due to the rotation of the rollers. In previous studies, only rolling motion in the radial direction has been considered [3-5]. In this study, along with rolling motion, sliding motion is also considered for accurate GAF estimation and, in order to analyze the friction characteristics in detail, the friction coefficient and rolling-sliding ratio which were experimentally obtained are employed.

The friction characteristics are determined by the friction coefficient, the rolling-sliding ratio, and the normal force. To analyze the friction characteristics

in detail, an analysis of the friction coefficient is required, and in general, the friction coefficient is determined by the main factors of the friction coefficient: the normal pressure, the sliding velocity and the viscosity. Therefore, the analysis of the main factors of the friction coefficient should be preceded.

2.3.1. Friction coefficient analysis

As mentioned above, the main factor of the friction are the normal pressure, sliding velocity and the viscosity. First, the normal pressure was analyzed.

Normal pressure

Normal pressure can be calculated from the geometry of CV joints and the contact areas. The contact points and the curvature can be also calculated geometrically and the contact areas of the contact points can be calculated by Hertz's law [21, 22].

The shape of contact areas depends on the contact types. In the case of the

contact between spherical rollers and tracks, the contact area is considered as an ellipse whereas it is considered as a rectangle in the contact between spherical rollers and needle rollers [18, 21]. Contact area can be calculated from the equation below.

$$E_{eq} = \left(\frac{1 - {\nu_1}^2}{E_1} + \frac{1 - {\nu_2}^2}{E_2} \right)^{-1} \quad (2.17)$$

where E_{eq} = equivalent Young's modulus, E_1 = Young's modulus of material 1, E_2 = Young's modulus of material 2, ν_1 = Poisson's ratio of material 1, ν_2 = Poisson's ratio of material 2.

Point contact

The equivalent radius of contact points depends on the contact types. When a

point contact occurs, the equivalent radius can be calculated by the following equations.

$$R_{eq1} = \left(\frac{1}{R_1} + \frac{1}{R_3}\right)^{-1} = \frac{R_1 R_3}{R_1 + R_3} \quad (2.18)$$

$$R_{eq2} = \left(\frac{1}{R_2} + \frac{1}{R_4}\right)^{-1} = \frac{R_2 R_4}{R_2 + R_4} \quad (2.19)$$

where R_{eq1}, R_{eq2} = equivalent radii of curvature, R_1, R_3 = radii of curvature of material 1, R_2, R_4 = radii of curvature of material 2.

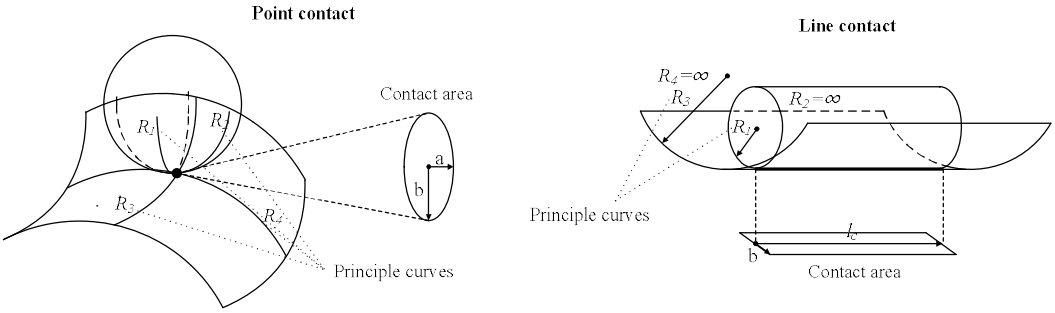

(a) **(b)**

Figure 2.7 Contact type (a) point contact (b) line contact

When one point contact occurs between two materials, as shown in Figure 2.7 (a), each material has two main radii of curvature. By calculating one radius from material 1 with the matching radius from material 2, the equivalent radius of curvature at the contact point can be obtained and two radii of curvature can be obtained from equation (2.18) and (2.19). From equation (2.17) – (2.19) and the equations presented in contact mechanics, the contact areas can be calculated as follows.

$$A_1 = \pi a^2 = \pi \sqrt[3]{\left(\frac{3NR_{eq1}}{4E_{eq}}\right)^2} \quad (2.20)$$

$$A_2 = \pi b^2 = \pi \sqrt[3]{\left(\frac{3NR_{eq2}}{4E_{eq}}\right)^2} \quad (2.21)$$

$$A = \sqrt{A_1 A_2} = \pi \sqrt[3]{\left(\frac{3N}{4E_{eq}}\right)^2 R_{eq1} R_{eq2}} \quad (2.22)$$

where A = contact area, a = minor radius of contact area in point contact, b = major radius of contact area in point contact.

Line contact

In the case of line contacts, each material has one main radius of curvature, so

they create one equivalent radius as shown in Figure 2.7 (b). In this case, the other equivalent radius is considered to be infinite. The equivalent radius and the contact areas are calculated by the following equations.

$$R_{eq} = \left(\frac{1}{R_1} + \frac{1}{R_3}\right)^{-1} = \frac{R_1 R_3}{R_1 + R_3} \quad (2.23)$$

$$A = 2bl_c = 2l_c\sqrt{\frac{2NR_{eq}l_c}{\pi E_{eq}}} \quad (2.24)$$

where b = width of contact area in line contact, l_c = length of contact area in line contact.

When normal loads and contact areas were obtained, normal pressure is

$$P = \frac{N}{A} \quad (2.25)$$

In the case of point contacts,

$$P = \pi \sqrt[3]{\left(\frac{4E_{eq}}{3}\right)^2 \frac{N}{R_{eq1}R_{eq2}}} \quad (2.26)$$

And in the case of line contacts,

$$P = \frac{1}{2l_c}\sqrt{\frac{\pi E_{eq} N}{2R_{eq} l_c}} \quad (2.27)$$

Sliding velocity

As mentioned previously, rolling-sliding motion and pure sliding motion occur between the spherical rollers and the tracks when a CV joint rotates as shown in Figure 2.8.

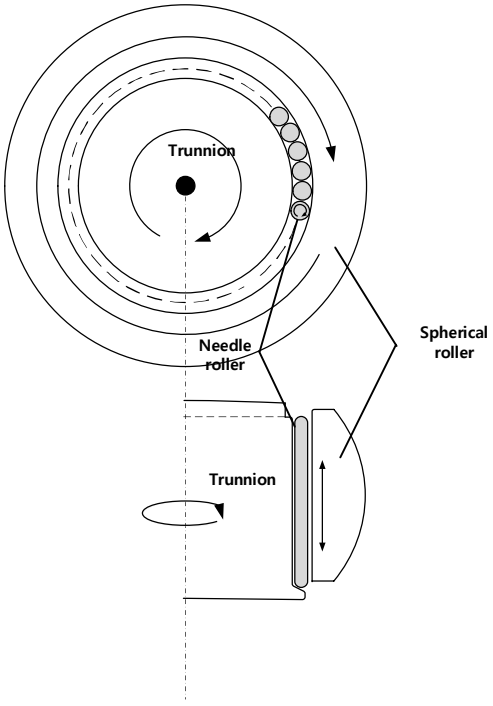

Figure 2.8 Relative motion of roller pair

For both motions, sliding velocity is one of the critical factors that determine friction characteristics. Besides the relative motion between spherical rollers and tracks, there is motion between needle rollers and adjacent components. In this study, this relative motion surrounding needle rollers was assumed to be pure sliding and have little influence on GAF because the values are very small and the motion runs under lubricated conditions. The motion between spherical rollers and needle rollers which occurs in the direction of trunnion axis is pure sliding and it can be represented by the following equation.

$$V_{ns} = \frac{PCR}{\cos\beta} \frac{\dfrac{1}{\cos\beta\sqrt{\cos^2(\tan^{-1}(\tan\varphi_{i+1}\cos\beta)+\psi)+\left(\frac{\sin(\tan^{-1}(\tan\varphi_{i+1}\cos\beta)+\psi)}{\cos\beta}\right)^2}} - \dfrac{1}{\sqrt{\cos^2(\tan^{-1}(\tan\varphi_i\cos\beta)+\psi)+\left(\frac{\sin(\tan^{-1}(\tan\varphi_i\cos\beta)+\psi)}{\cos\beta}\right)^2}}}{t} \quad (2.28)$$

where t = time, V_{ns} = sliding velocity between needle roller and spherical roller.

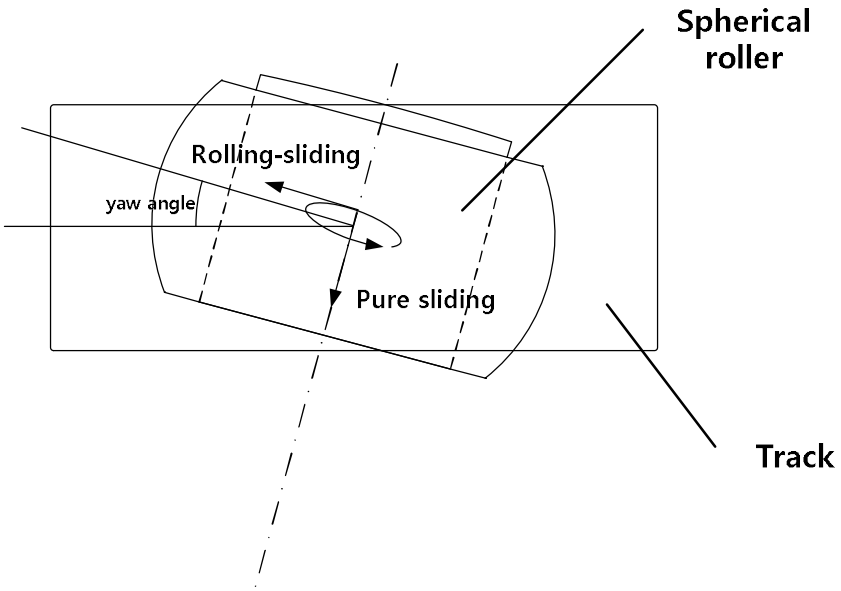

Figure 2.9 Motion of spherical roller

In the case of the sliding velocity between spherical rollers and tracks, pure sliding motion and rolling-sliding motion occur at the same time. In this case, as shown in Figure 2.9, sliding motion occurs in the direction of trunnion axis whereas rolling-sliding motion occurs in the direction of the tangential direction of spherical rollers. For rolling-sliding motion, the translation velocity of

spherical rollers can be calculated by the following equation.

$$V_t = \frac{\dfrac{PCR^2 \tan\beta \cos(\tan^{-1}(\tan\varphi_{i+1}\cos\beta)+\psi)}{\sqrt{(PCR\cos(\tan^{-1}(\tan\varphi_{i+1}\cos\beta)+\psi))^2+\left(\frac{PCR}{\cos\beta}\sin(\tan^{-1}(\tan\varphi_{i+1}\cos\beta)+\psi)\right)^2}} - \dfrac{PCR^2 \tan\beta \cos(\tan^{-1}(\tan\varphi_i\cos\beta)+\psi)}{\sqrt{(PCR\cos(\tan^{-1}(\tan\varphi_i\cos\beta)+\psi))^2+\left(\frac{PCR}{\cos\beta}\sin(\tan^{-1}(\tan\varphi_i\cos\beta)+\psi)\right)^2}}}{t} \quad (2.29)$$

where V_t = translation velocity of spherical roller.

Actual sliding velocity on the contact point of rolling-sliding motion is a product of rolling –sliding ratio and translation velocity.

$$V_s = \gamma V_t \quad (2.30)$$

where V_s = actual sliding velocity of spherical roller.

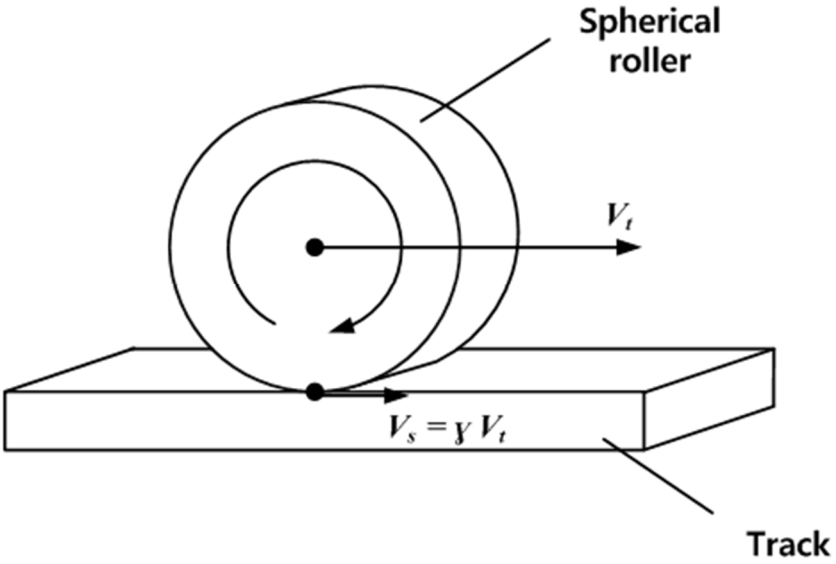

Figure 2.10 Relative sliding velocity between spherical roller and track

As mentioned previously, the rolling-sliding motion was not considered in previous researches. However, GAF caused by the rolling-sliding motion is considerable. Therefore, detailed analysis of rolling-sliding motion is required. In this study, the rolling-sliding motion was analyzed in detail and the actual sliding velocity was derived by using the equation (2.30). The calculated results are shown in Figure 2.11. In the results, the rolling-sliding ratio is based on results of

experimental analysis from the later section.

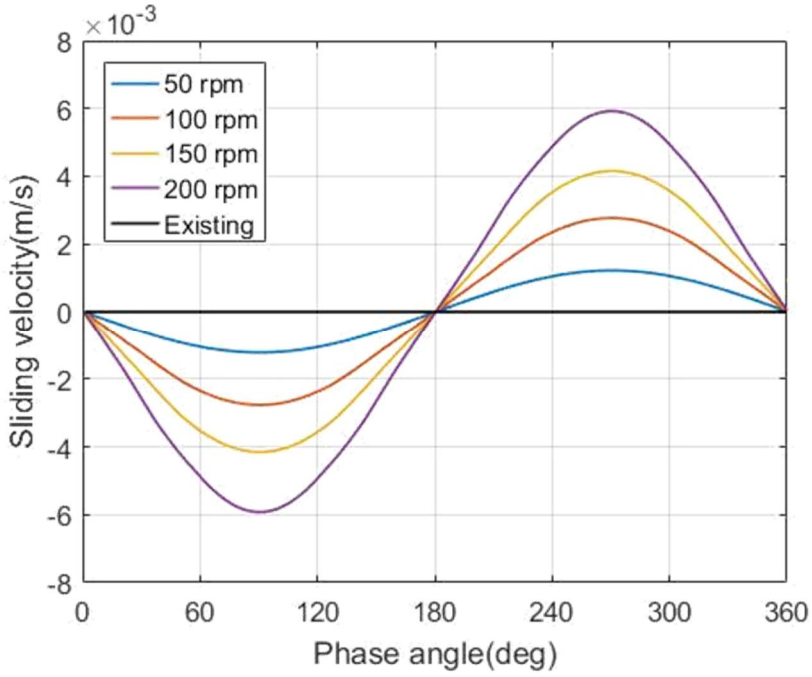

Figure 2.11 Actual sliding velocity of rolling-sliding motion

As shown in Figure 2.11, the actual sliding velocity of the rolling-sliding motion increases as the rotational speed of the constant velocity joint increases.

The actual sliding speed has a maximum value when the phase angle is 90 degrees, a minimum value when the phase angle is 270 degrees, and 0 when the phase angle is 0,180 and 360 degrees.

Viscosity

CV joints run under lubricated conditions. In order to verify the friction model by experimenting it and estimate GAF accurately, the same lubricant as the one used in experimenting the CV joint was employed. In addition to viscosity, temperature was also controlled to be the same as the temperature in the CV joint so that the experiments could be controlled under consistent lubricated conditions [23]. The properties of the lubricant are as shown in TABLE 2.2.

TABLE 2.2 Properties of lubricant

Composition	Polyurea, mineral oil, etc.
Viscosity @ 40 °C (mm^2/s)	100
Viscosity @ 100 °C (mm^2/s)	11
Available temperature range (°C)	-30 ~ +180
Flash point (°C)	250

Friction coefficient measurement

In this study, a tribometer is set up to measure the friction coefficients of CV joint components. It is a pin-on-disk type and the disk is rotated by a servo motor as shown in Figure 2.12. Normal load is applied by weights. The friction force between the pin and the disk is converted to torque which is measured by a torque sensor. Consequently, friction coefficients can be calculated from the torque and the normal load.

The tests are performed with various normal loads and sliding velocities to identify the relationship between friction coefficient and its factors – sliding velocity and normal pressure. Normal pressure is calculated from normal load by Hertz's Law. Sliding velocity is controlled by the servo motor. The same lubricant as the one in the target CV joint was used. The characteristics of the lubricant used in this study are shown in TABLE 2.2. Temperature is controlled to maintain the same as the actual driving conditions of the target CV joint. The experiment conditions are shown in TABLE 2.3.

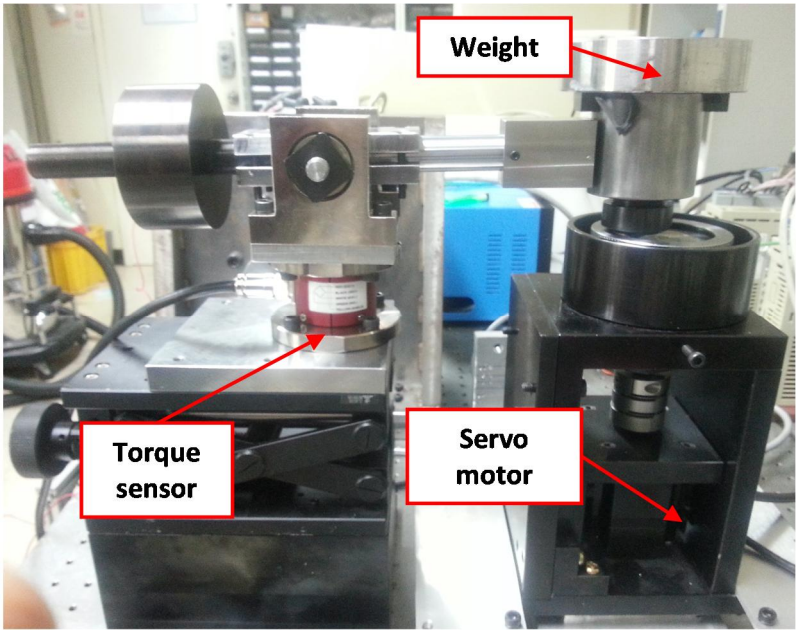

Figure 2.12 Tribometer

TABLE 2.3 Measurement conditions of friction coefficient

Normal load (N)	60, 65, …, 130
Sliding velocity (m/s)	0.001, 0.002, …, 0.085
Temperature (°C)	40 ~ 45

Friction coefficients measured by the tribometer are shown in Figure 2.13.

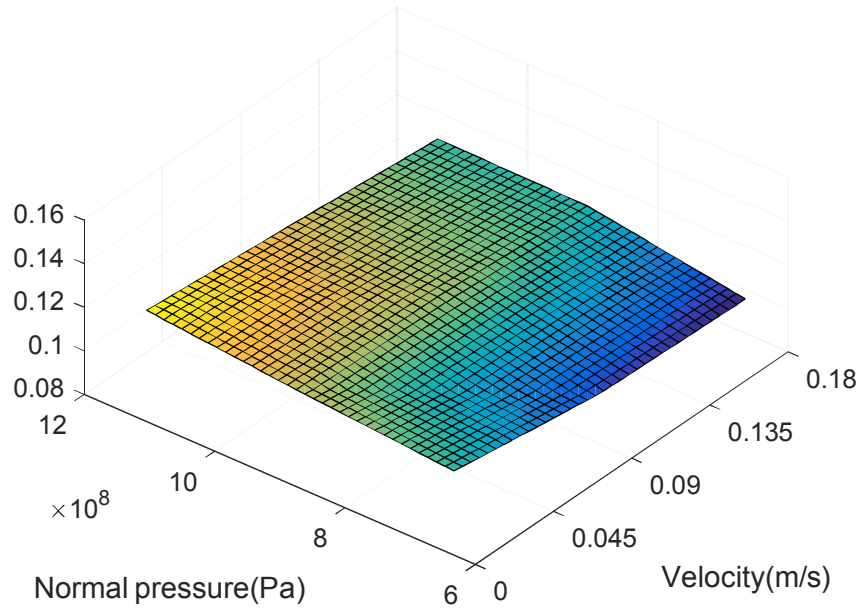

(a)

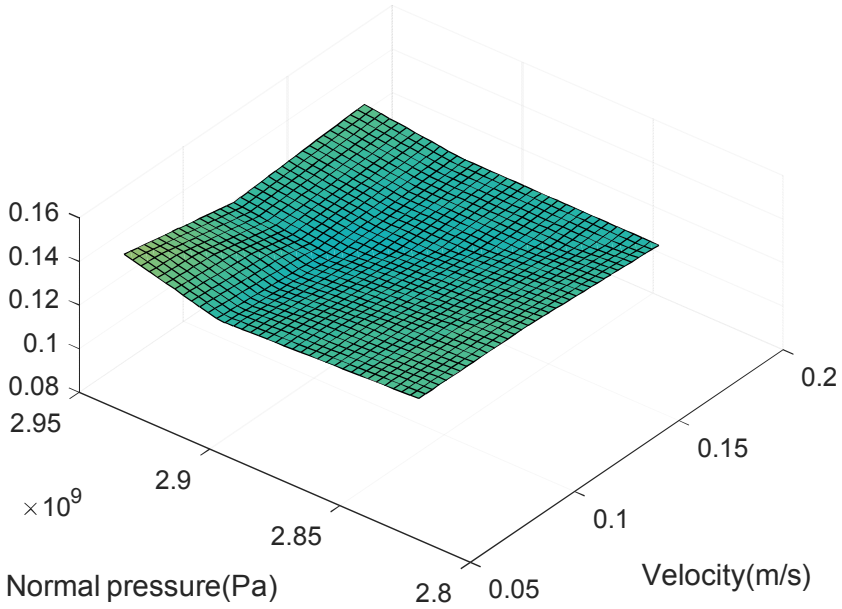
0.16
0.14
0.12
0.1
0.08
2.95
2.9
2.85
2.8
×10^9
Normal pressure(Pa)
0.05
0.1
0.15
0.2
Velocity(m/s)

(b)

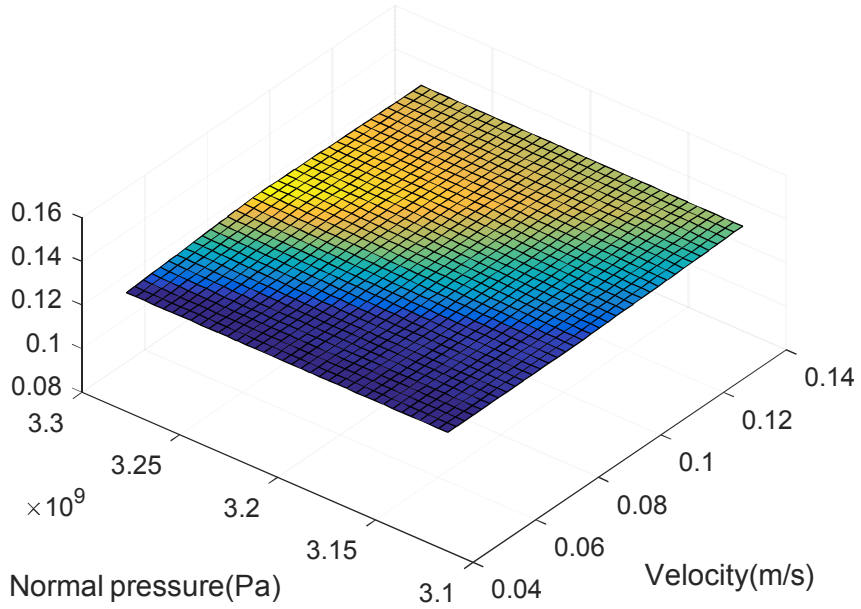

(c)

Figure 2.13 Friction coefficients between (a) spherical roller and track (b) spherical roller and needle roller (c) needle roller and trunnion

Since the main cause of the GAF is the friction between the spherical roller and the track, the friction coefficient of the spherical roller and the track is further measured by subdividing the temperature.

In this study, since the GAF was measured by dividing the torque condition from 100 to 400 Nm, the friction coefficient was measured at the corresponding temperature range from 22 to 45 °C. The conditions of the normal pressure and the sliding velocity are same as TABLE 2.3. The results are shown in Figure 2.14.

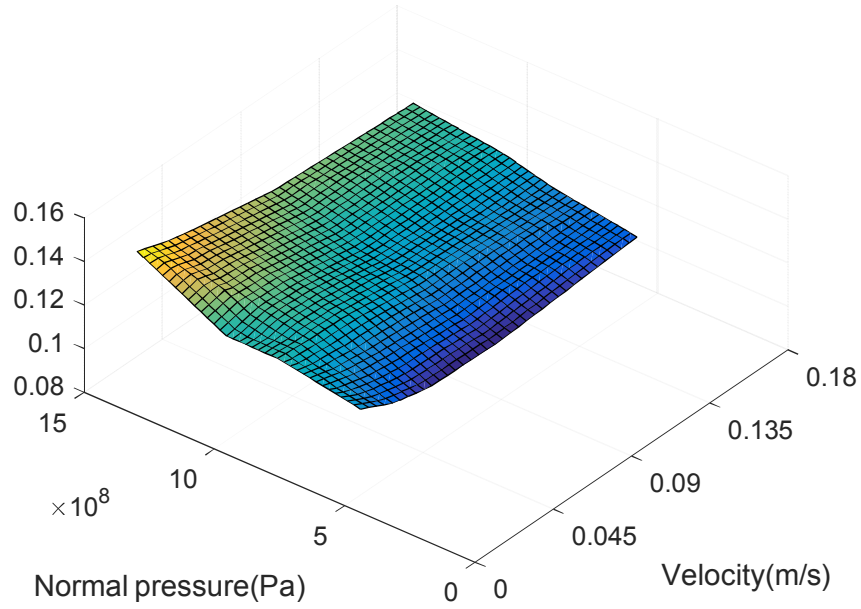
0.16
0.14
0.12
0.1
0.08
15
10
×10^8
5
0
Normal pressure(Pa)
0
0.045
0.09
0.135
0.18
Velocity(m/s)

(a)

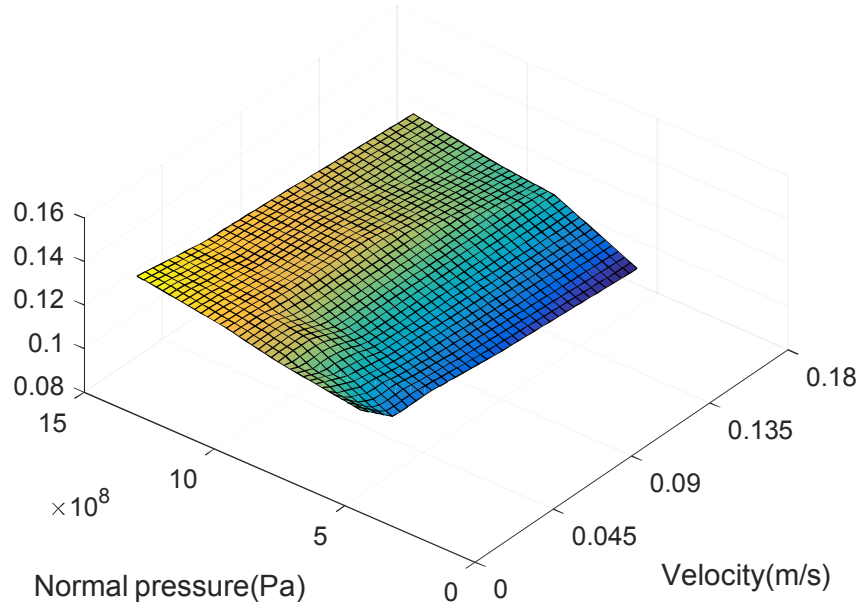

(b)

Figure 2.14 Friction coefficients between spherical roller and track at temperature of (a) 22 °C and (b) 32 °C

As shown in Figure 2.13 and Figure 2.14, the friction coefficient increases as the pressure increases and decreases as the velocity increases in all conditions. Also, as the temperature increases, the friction coefficient increases.

2.3.2. Pure sliding friction analysis

GAF is mainly generated by friction between the spherical roller and the track. As shown in Figure 2.9, the main relative motions between the spherical roller and the track are pure sliding motion in the direction of trunnion axis and the rolling-sliding motion in the tangential direction of the spherical roller. Therefore, the pure sliding friction and the rolling-sliding friction have to be analyzed.

First, the pure sliding friction force applied to the motion in the direction of trunnion axis can be obtained by the following equation.

$$F_s = \mu_s N_{st} \quad (2.31)$$

where F_s = sliding friction force between spherical roller and track, μ_s = sliding friction coefficient, N_{st} = normal force between spherical roller and track.

The pure sliding friction coefficients were measured in the previous part. The pure friction coefficient map was applied to the pure sliding friction characteristics analysis and the normal force was calculated from the driving conditions.

2.3.3. Rolling-sliding friction analysis

The rolling-sliding friction model applied to the tangential direction of spherical roller can be obtained by the following equations.

$$F_{rs} = \mu_{rs} N_{st} \quad (2.32)$$

$$\mu_{rs} = \gamma \mu_s \quad (2.33)$$

$$\gamma = \frac{l_s}{l_t}, \qquad 0 \leq \gamma \leq 1 \tag{2.34}$$

$$\mu_{rs} = \frac{l_s}{l_t}\mu_s \tag{2.35}$$

where F_{rs} = rolling-sliding friction force between spherical roller and track, μ_{rs} = rolling-sliding friction coefficient, γ = rolling-sliding ratio, l_t = entire moving distance of roller center on the surface of track, l_s = pure sliding distance of roller on the surface of track.

Rolling-sliding friction coefficient can be assumed to be the product of rolling-sliding ratio and sliding friction coefficient as shown in equation (2.33) [19, 24]. In the case of rolling-sliding ratio, it is very hard to estimate the ratio because it highly depends on the driving conditions of CV joints. Therefore, in this study, rolling-sliding ratio is experimentally studied for accurate GAF estimation.

Friction coefficient, on the other hand, varies with the factors such as normal pressure, sliding velocity and viscosity [25, 26]. In this study, these factors were considered and applied to a tribometer to acquire friction coefficients at various driving conditions.

Rolling-sliding ratio

As mentioned earlier, Rolling-sliding motion of spherical rollers occurs as they move along the tracks. This motion has much influence on GAF so this study takes this motion into account for GAF estimation. A rolling-sliding ratio measurement system shown in Figure 2.15 was set up to measure the rolling-sliding ratio between spherical rollers and tracks. A servo motor makes relative motion between the spherical rollers and the tracks. The angle between the stage and the weight bar is the same as the angle between the spherical rollers and the tracks. The side of the spherical roller is marked by Yb-doped fiber laser and a

high speed camera films the number of rotation of the rollers. By dividing the total travelling distance by their rolling distance, the rolling-sliding ratio can be obtained. In order to apply various normal loads to the roller, weights are placed at the end of the weight bar.

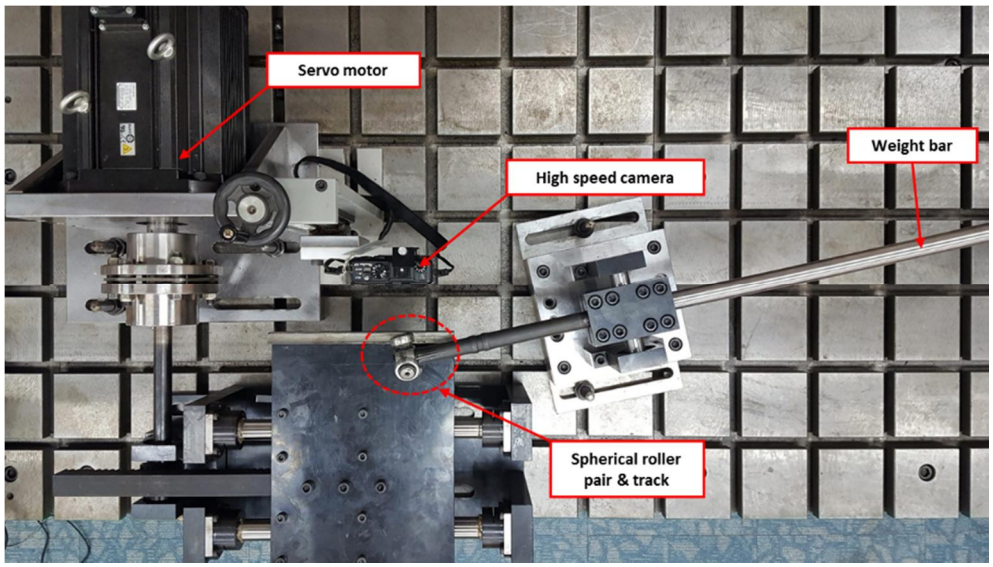

(a)

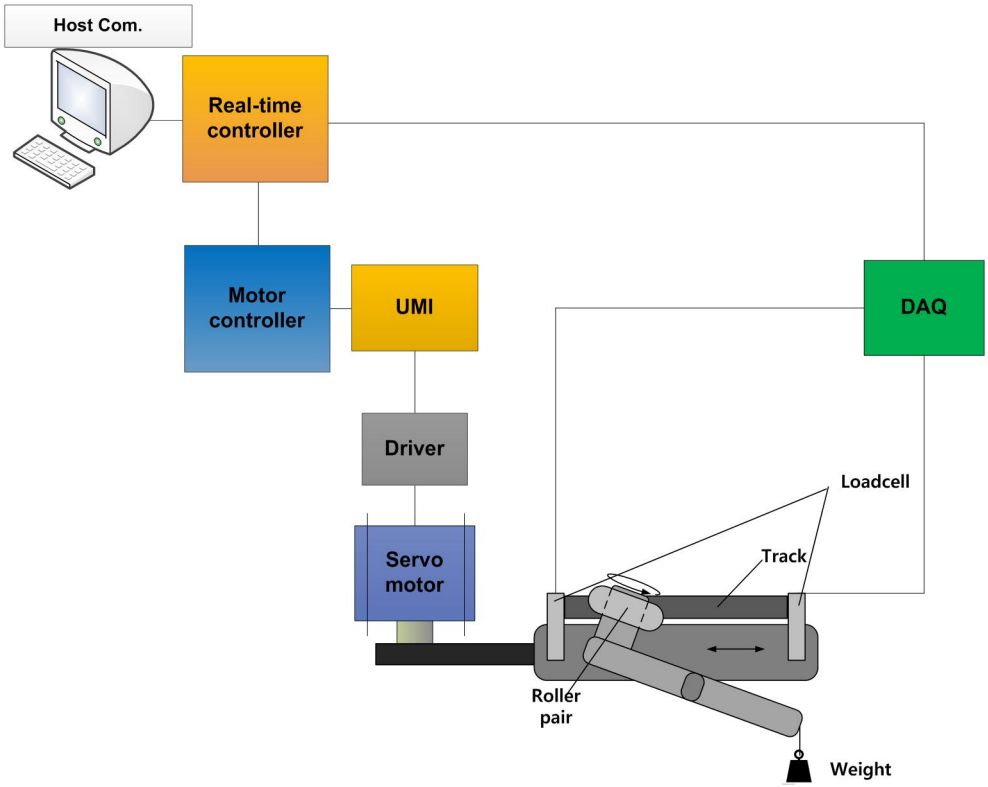

(b)

Figure 2.15 Experimental setup for rolling-sliding ratio measurement: (a) the actual measurement system (b) schematic diagram of the system

A rolling-sliding friction characteristics are analyzed based on pure sliding friction characteristics because the friction coefficient of rolling-sliding motion is

determined by rolling-sliding ratio and the translation velocity of spherical roller as mentioned previously. Rolling-sliding ratio measured by the rolling-sliding measurement system is described in Figure 2.15.

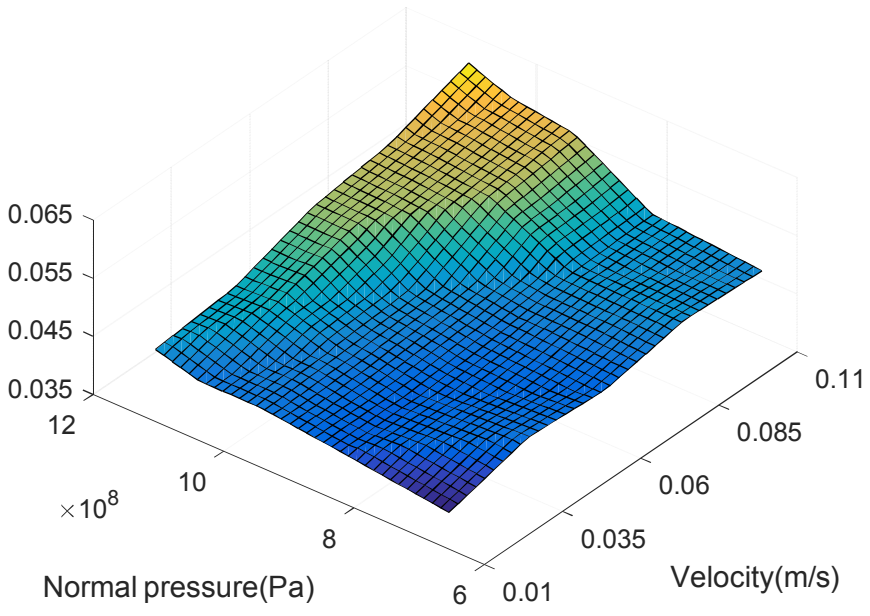

Figure 2.16 Rolling-sliding ratio between spherical roller and track

Figure 2.16 shows rolling-sliding ratio with respect to normal pressure and

translation velocity. As known from the figure, rolling-sliding ratio increases with the increase of normal pressure and translation velocity. It reaches the maximum value of 0.0601 when normal pressure and translation velocity are the maximum whereas it reaches the minimum value of 0.0413 when normal pressure and translation velocity are the minimum.

Rolling-sliding friction coefficient is the product of rolling-sliding ratio and sliding friction coefficient as shown in equation (2.33) [19, 24]. Therefore, rolling-sliding friction coefficient can be obtained as shown in Figure 2.17. As rolling-sliding ratio, rolling-sliding friction coefficient also increases with the increase of normal pressure and velocity. It reaches the maximum value of 0.0074 when normal pressure and velocity are the maximum values while it reaches the minimum value of 0.0049 when normal pressure and velocity are the minimum. From all of the results above, the friction model of CV joints can be completely developed.

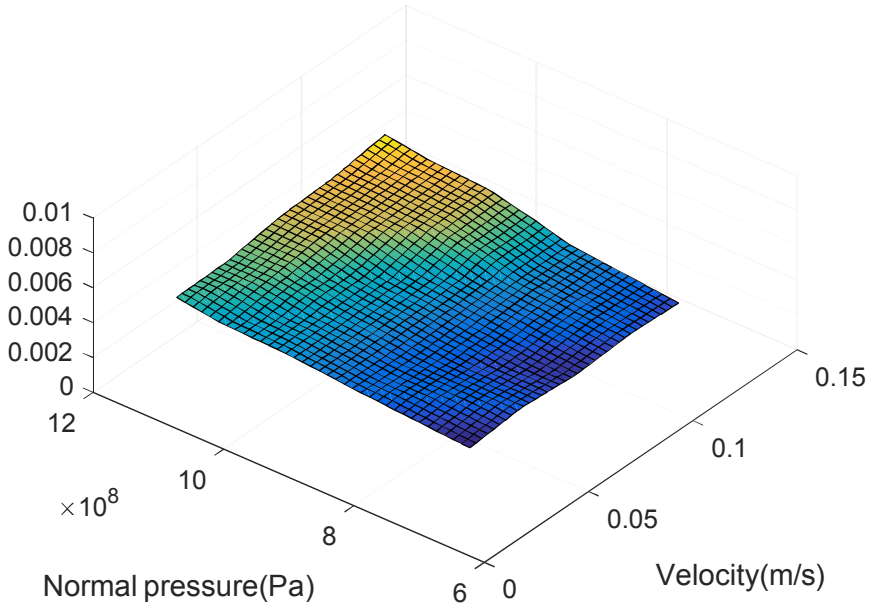

Figure 2.17 Rolling-sliding friction coefficient between spherical roller and track

2.4. GAF estimation model

Throughout the previous chapters, the kinematic analysis, the normal load derivation and the friction model development have been performed, which are

required to establish a GAF model of tripod type CV joints.

A tripod type CV joint has three spherical rollers which make reciprocal motion on each track. As they move along the tracks, each spherical roller generates axial force which varies with phase angle, and the sign of GAF is determined by the moving direction of rollers and yaw angles as shown in Figure 2.18. By applying friction characteristics and normal load to the geometry, the GAF model can be obtained.

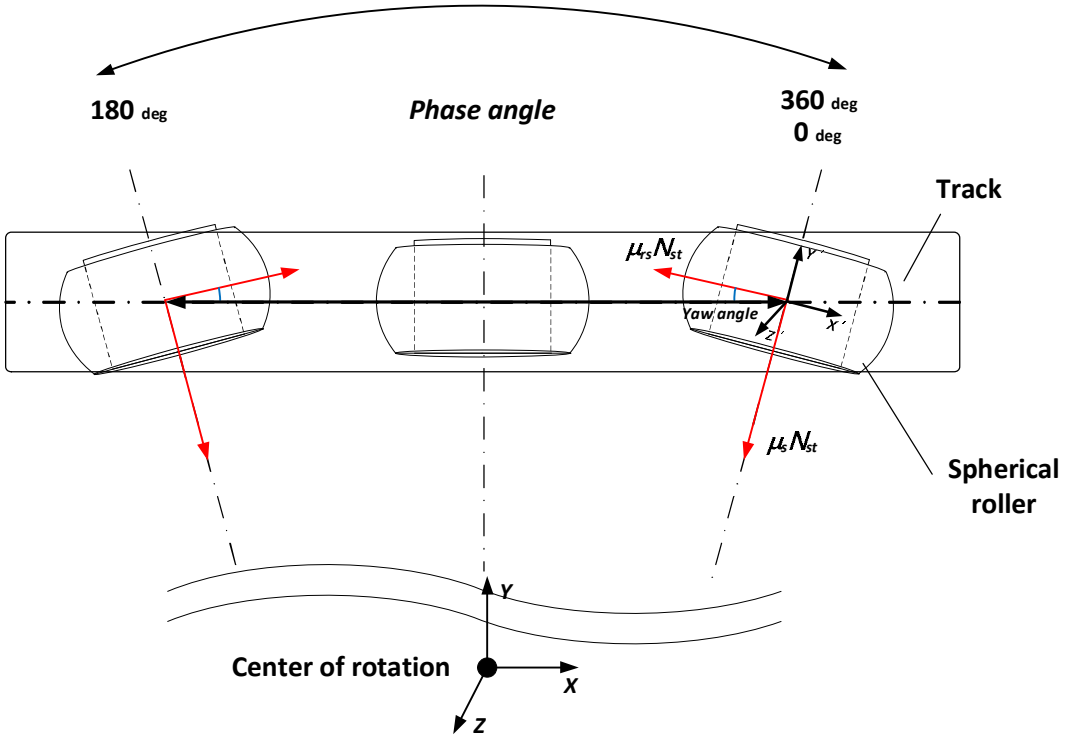

Figure 2.18 Relative motion between roller and track

$$GAF = \sum_{i=1}^{3} \mu_s N_{st} sin(\propto_i) sign|V_{t\_z}| + \mu_{rs} N_{st} cos(\propto_i) sign|V_{t\_x}| + f_a(T, rpm) \quad (2.36)$$

The first term of the equation represents the sliding friction force generated by

the motion in the direction of the trunnion axis between spherical rollers and tracks. The second term of the equation represent the rolling-sliding friction force in the tangential direction of spherical rollers.

The sign terms are determined by the relative motion between spherical rollers and tracks. They are positive when spherical rollers move toward the positive direction of Z (or X) axis while they are negative when the rollers move toward the negative direction of Z (or X) axis. The third term of the equation represents the moment of inertia which are determined by the mass and velocity of CV joints.

As mentioned previously, this study considers rolling-sliding motion and pure sliding motion and therefore, GAF is calculated from both motions. As shown in the second term of equation (2.36), rolling-sliding motion is the product of friction coefficient of pure sliding motion and rolling-sliding ratio. In this term, the rolling-sliding ratio is in the range from 0 to 1 and therefore, the friction coefficient of the rolling-sliding motion is smaller than that of the pure sliding

motion. Rolling-sliding ratio depends on driving conditions and it is very difficult to predict theoretically. Therefore, this study employs an empirical friction characteristics by applying rolling-sliding ratio obtained experimentally above.

2.5. Estimation result and verification

In this study, the friction characteristics were analyzed in detail and it was applied to the GAF model. In the friction characteristics analysis, mainly two friction characteristics were analyzed – pure sliding friction characteristics and rolling-sliding friction characteristics. In order to analyze the friction characteristics, friction coefficient and rolling-sliding ratio were analyzed experimentally. Unlike other studies, this study considered the rolling-sliding ratio. It is difficult to analyze rolling-sliding ratio because a new measurement system is needed and the measurement results have to be organized. By using the developed GAF model of the target CV joint the estimated results are shown in Figure 2.19.

The results are the GAF of 1 roller so as to compare the GAF of pure sliding friction with that of the rolling-sliding friction.

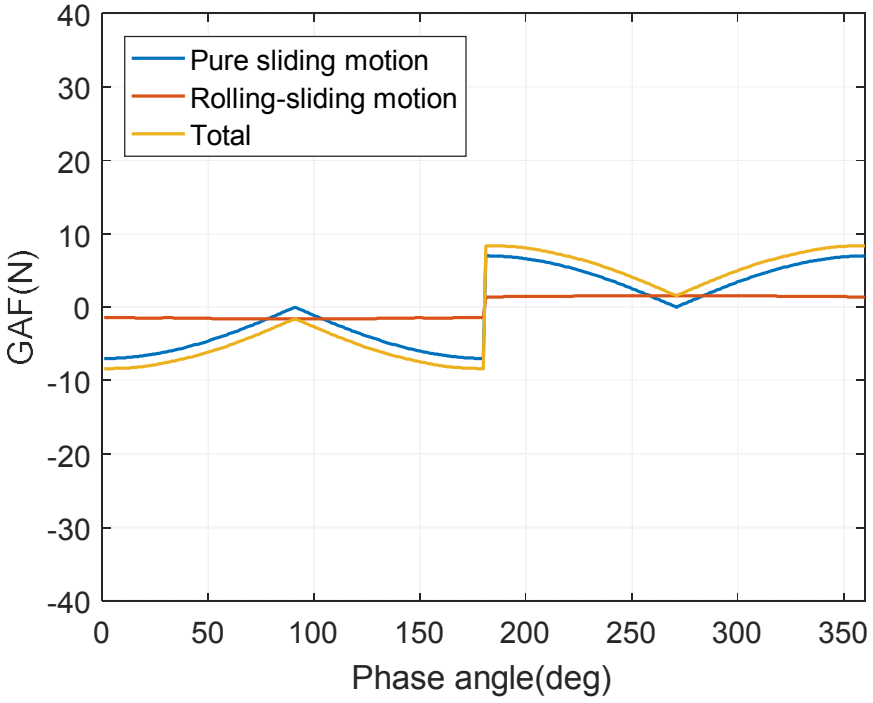

(a)

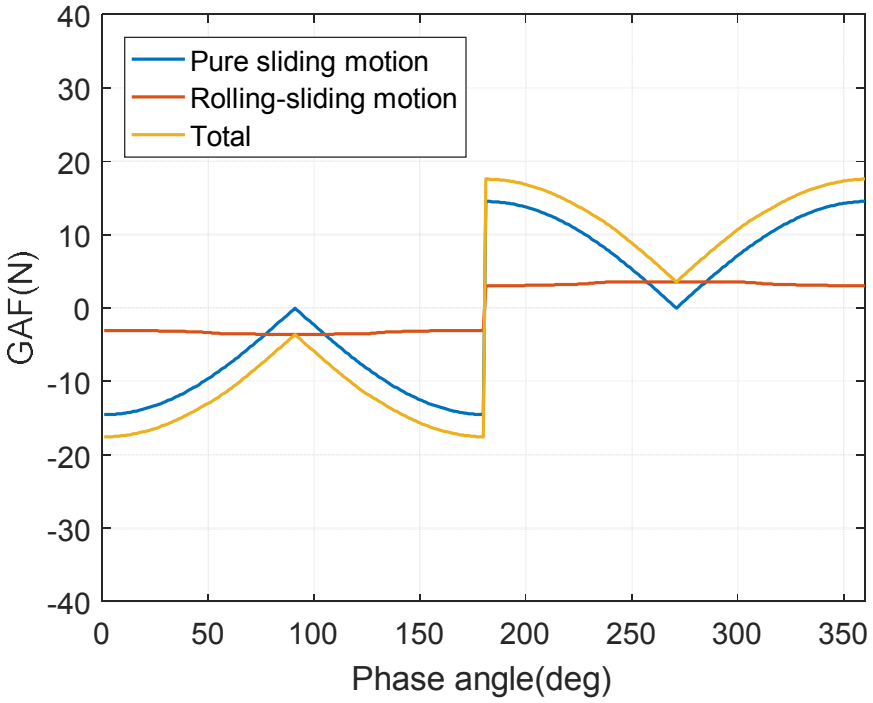
Pure sliding motion
Rolling-sliding motion
Total
GAF(N)
Phase angle(deg)
40
30
20
10
0
-10
-20
-30
-40
0
50
100
150
200
250
300
350

(b)

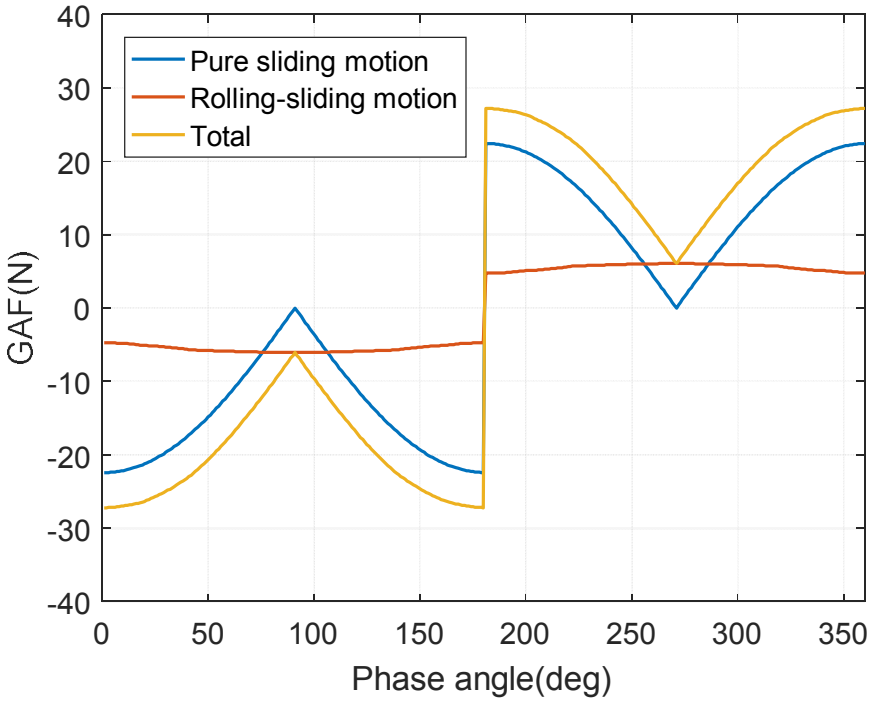
Pure sliding motion
Rolling-sliding motion
Total
GAF(N)
Phase angle(deg)
40
30
20
10
0
-10
-20
-30
-40
0
50
100
150
200
250
300
350

(c)

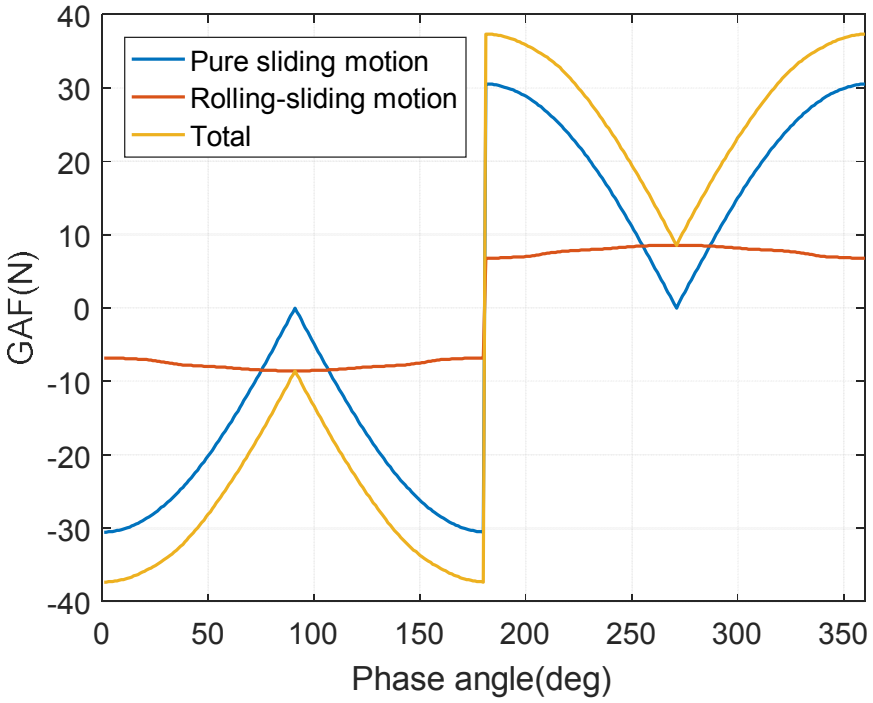

(d)

Figure 2.19 GAF estimation results of 1 roller according to the torque (a) 100 Nm (b) 200 Nm (c) 300 Nm (d) 400 Nm

As shown in Figure 2.19, total GAF which is sum of the GAF generated by the pure sliding friction and the GAF generated by the rolling-sliding friction increases as the increase of the torque. The gap between the total GAF and the

GAF of the pure sliding friction increase with the increase of the torque. It means that the bigger the torque, the greater the importance of the GAF generated by the rolling-sliding friction. In most previous studies, GAF generated by rolling-sliding friction was not consider.

The actual GAF of the tripod type CV joint is the sum of GAF of three rollers. The GAF of the target CV joint estimated by the GAF model is shown in Figure 2.20. Figure 2.20 (a) shows GAF at 400 Nm with respect to rotation speed and articulation angle. As shown, GAF increases with the increase of articulation angle but it does not show much difference with the increase of rotation speed. Figure 2.20 (b) shows GAF at 200 rpm with respect to resistance torque and articulation angle. Regardless of resistance torque, GAF increases with the increase of articulation angle. In addition to its increase trend, the higher the resistance torque is, the more critical the articulation angle is. At 100 Nm, GAF is in the range from 0 to 13.45 N whereas it is in the range from 0 to 59.21 N at 400 Nm. At 3 degrees of articulation angle, GAF is 4.42 N at 100 Nm and 20.16 N at

400 Nm, which has the difference of 15.74 N. At 12 degrees of articulation angle, on the other hand, GAF is 13.45 N at 100 Nm and 59.21 N at 400 Nm, which has the difference of 45.76 N.

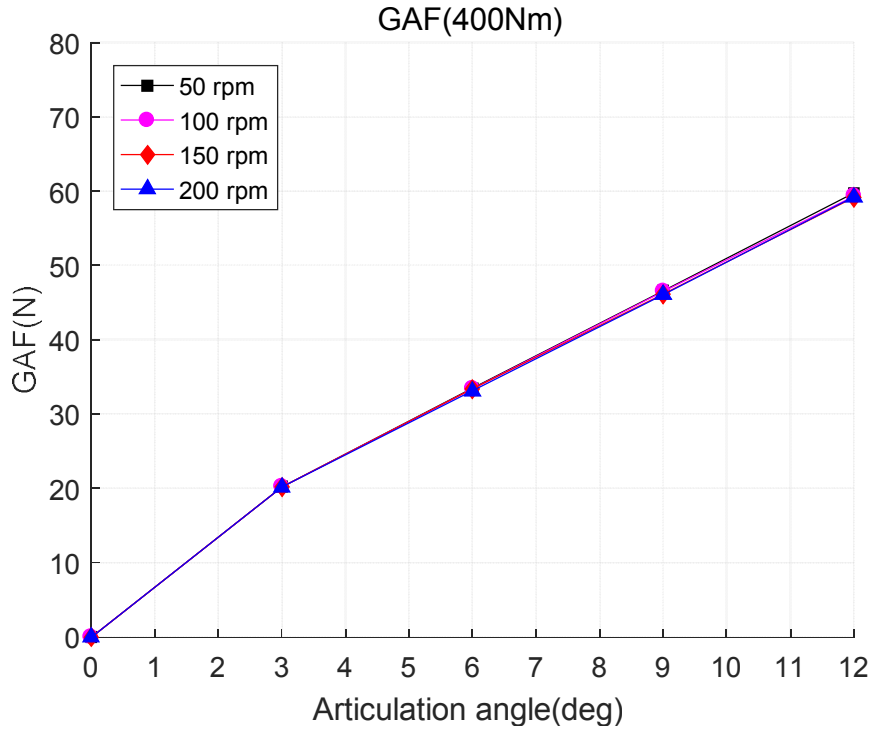

(a)

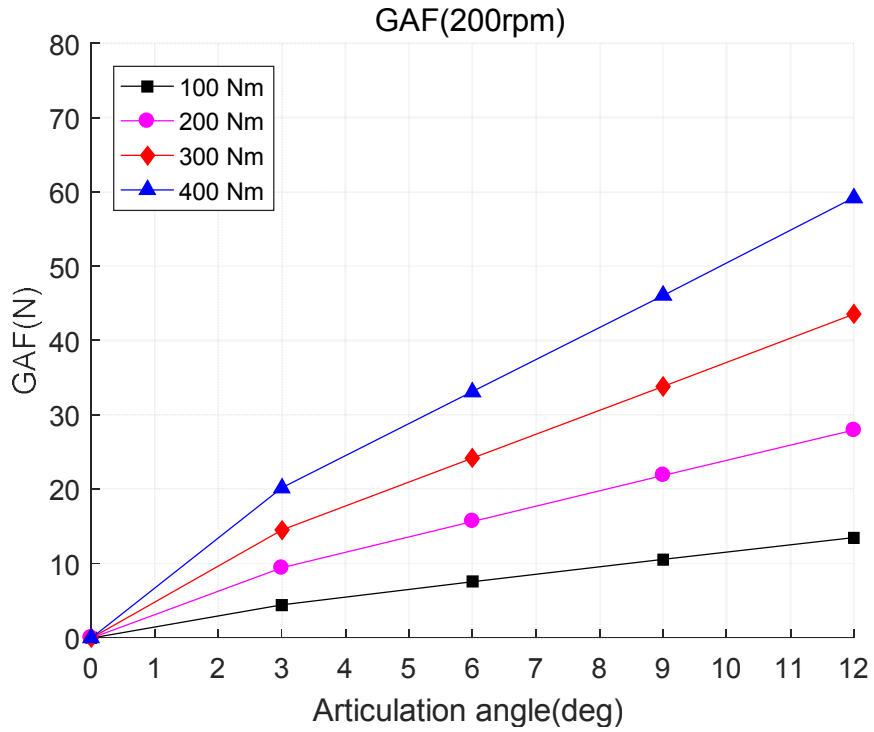

(b)

Figure 2.20 GAF estimation results according to change of (a) rpm (b) torque

In order to verify the estimated results, a GAF measurement system was set up in this study. As shown in Figure 2.21, two servo motors are connected at each end of the system. The drive motor applies angular velocity to the CV joint and the resistance motor applies resistant torque. Torque and force sensors locate

between the CV joint and the motors so that they can measure torque and axial force, respectively. Based on the theoretical analysis on kinematics and normal load, the torque measured by the torque sensor can be converted to normal pressure so experimental conditions can be controlled to correspond to the actual driving conditions. GAF from the axial force sensor is saved according to the driving conditions. The system was programmed with MATLAB and Labview and the experimental conditions are same as shown in TABLE 2.1.

In this study a new FFT model was developed to analyze the measured data. Process of analyzing the measured data is as shown in Figure 2.22 by using the FFT model. The raw data is converted to magnitude of 3rd order axial force by FFT model. The magnitude of 3rd order axial force is GAF because tripod type CV joint has three rollers. By using the FFT model, the data was classified.

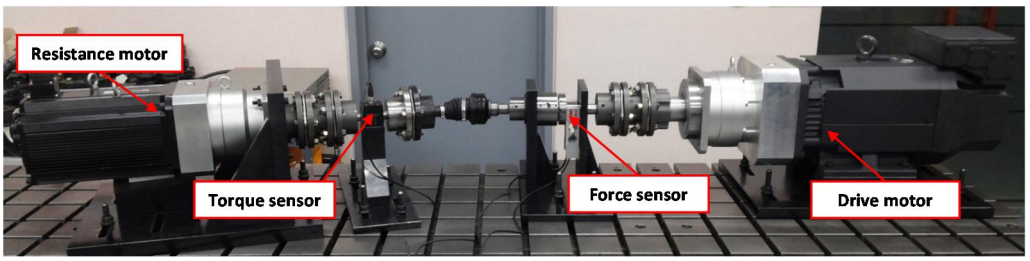

(a)

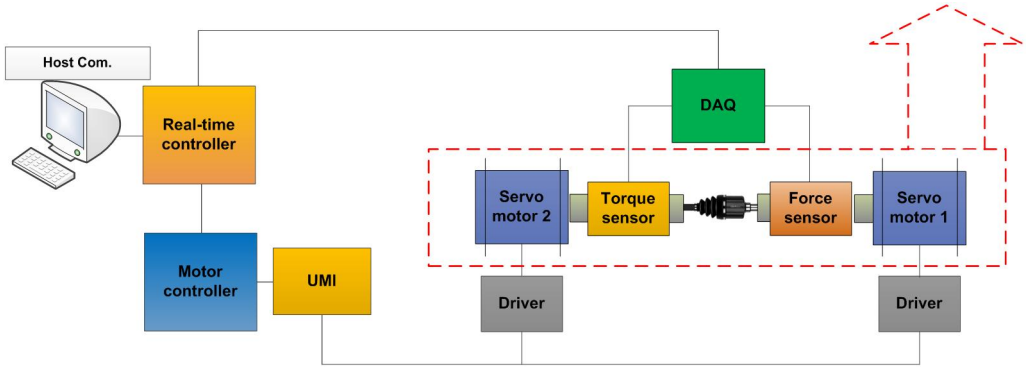

(b)

Figure 2.21 Experimental setup for GAF measurement: (a) the system on surface table and (b) schematic diagram of the system

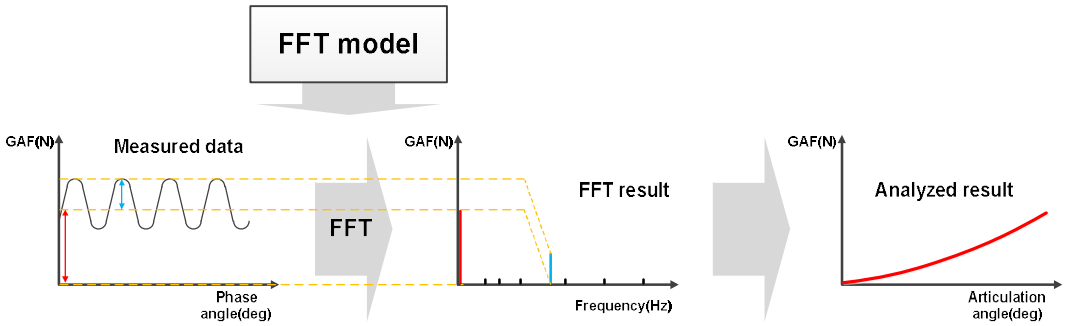

Figure 2.22 Process of analyzing raw data using FFT model

As the final procedure of this study, the GAF estimation results are verified by comparing the estimated results with the experimental results. All conditions of the experiments were the same as the GAF simulation conditions. The comparison results are as follows.

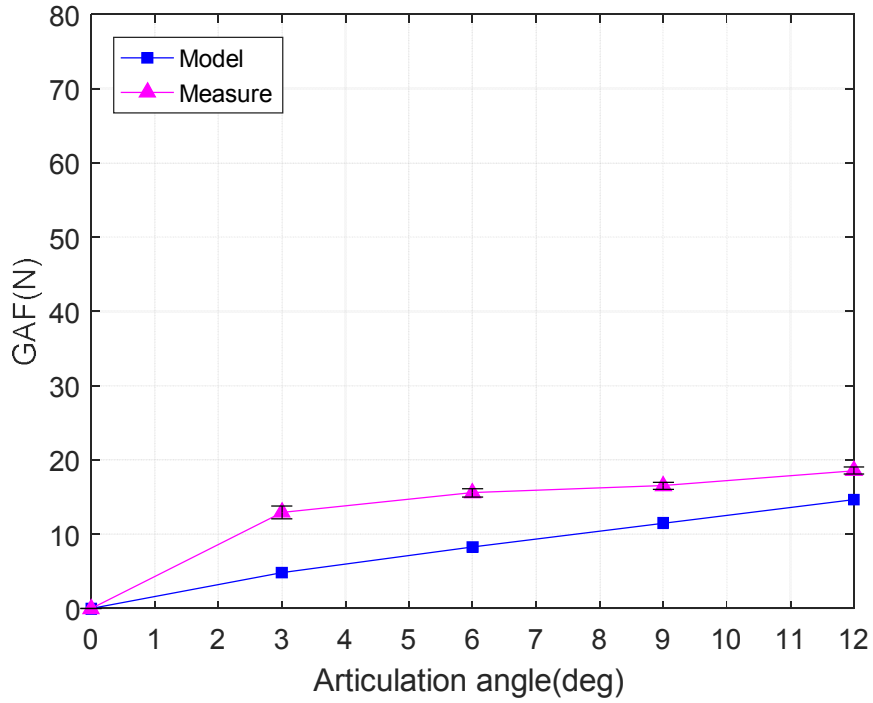
Model
Measure
GAF(N)
Articulation angle(deg)
0
10
20
30
40
50
60
70
80
0
1
2
3
4
5
6
7
8
9
10
11
12

(a)

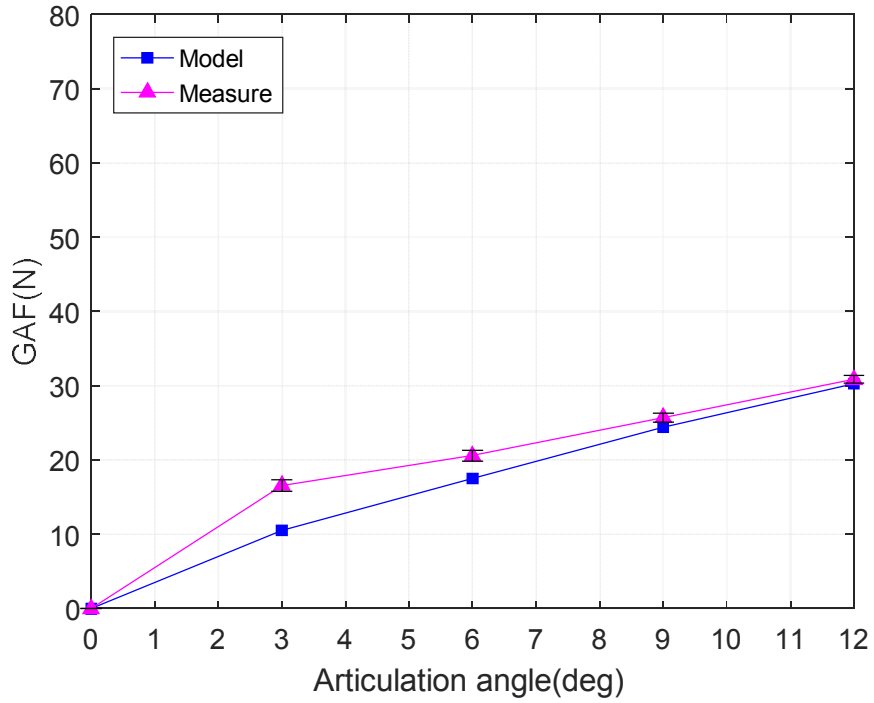
Model
Measure
GAF(N)
Articulation angle(deg)
0
10
20
30
40
50
60
70
80
0
1
2
3
4
5
6
7
8
9
10
11
12

(b)

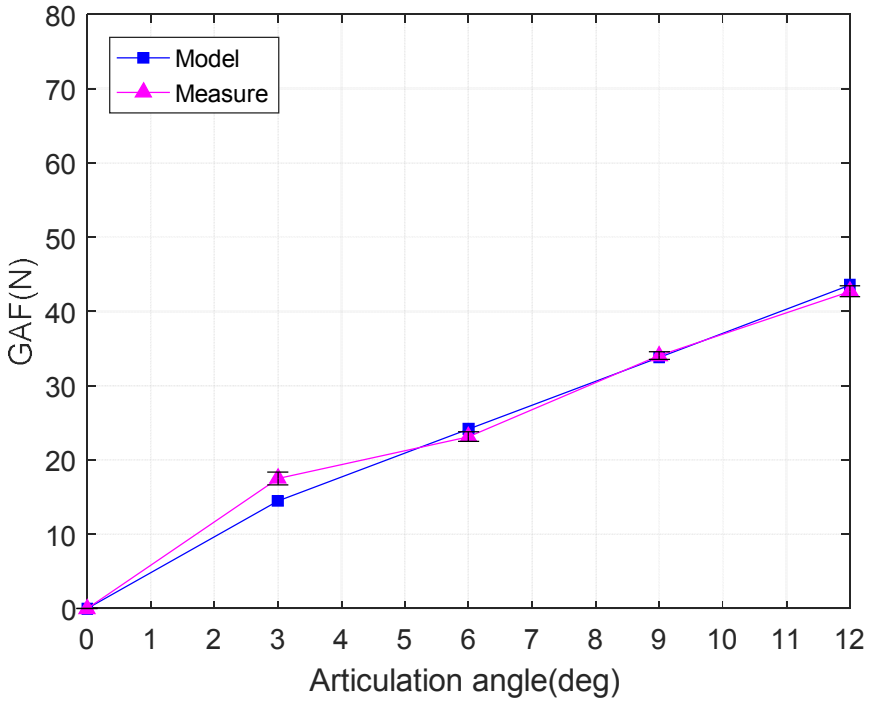
Model
Measure
GAF(N)
Articulation angle(deg)
0
10
20
30
40
50
60
70
80
0
1
2
3
4
5
6
7
8
9
10
11
12

(c)

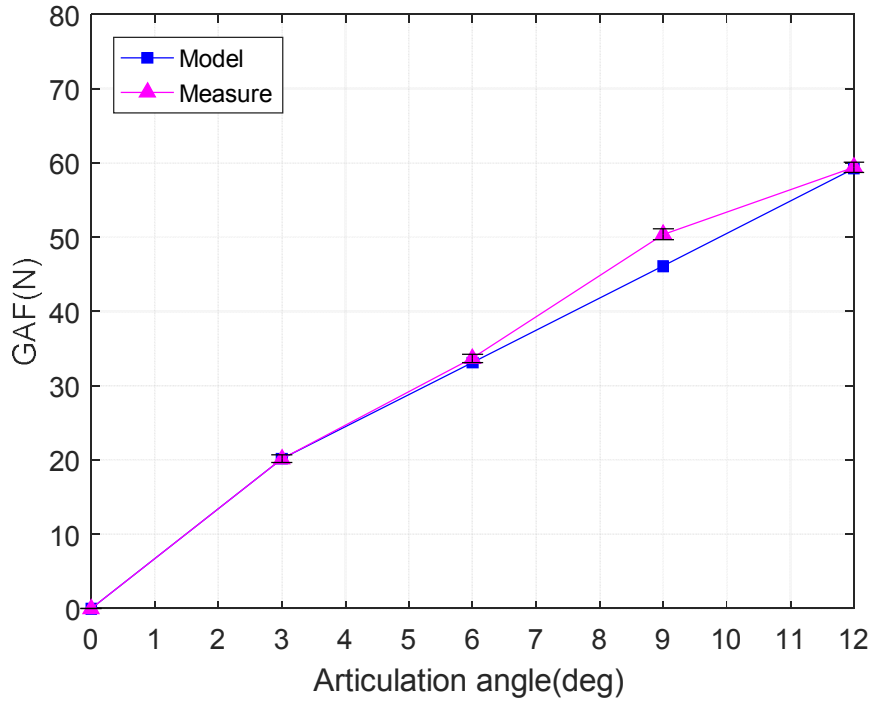

(d)

Figure 2.23 GAF verification (200 rpm) according to change of torque (a) 100 Nm (b) 200 Nm (c) 300 Nm (d) 400 Nm

Figure 2.23 shows the verification results at 200 rpm with respect to resistance torque. The measured is the average value of 5 experiment results. As shown in Figure 2.23 (a), the difference between estimation and measurement decreases

with the increase of articulation angle. The largest difference is 8.56 N at 3 degrees of articulation angle. As resistance torque increases, the difference between estimation and measurement reduces, which means the GAF model provides more accurate estimation. Especially at 300 and 400 Nm, GAF model gives very accurate estimation results. The difference between the measured data and the estimated data at low torque conditions is caused by difference of temperature between measurement condition and estimation condition. However, the difference is small.

Chapter 3

3. GAF reduction using GAF estimation model

In the previous chapter, a new GAF estimation model was developed and it was verified by a GAF measurement system. In this chapter, GAF factors were analyzed by using the verified GAF model. Based on the GAF factor analysis, sensitivity analysis of the GAF factors was performed, and the GAF according to the GAF factor changes was predicted accordingly. Based on the results, direction of GAF reduction was suggested. Next, prototypes which have changed parameters were manufactured and the GAF was measured through a GAF measurement system. Then, the results of the previous estimation was verified by the measured results. Finally, the reduction of the GAF was achieved.

3.1. Sensitivity analysis of GAF factors

In the GAF model developed above, the main factors directly affecting the GAF are the friction coefficient and the normal force. Since the normal force is influenced by the driving condition, the GAF was analyzed through the analysis of the friction coefficient. As can be seen from equation (2.36), the GAF consists of the pure sliding term and the rolling-sliding term. The rolling-sliding ratio is also a major factor in the GAF because the rolling-sliding term is composed of the rolling-sliding ratio and the pure sliding friction coefficient. Therefore, it is necessary to analyze the pure sliding friction coefficient and the rolling-sliding ratio.

As shown in equation (2.36), the pure sliding friction coefficient and the rolling-sliding ratio are affected by the normal pressure and the sliding velocity. As the normal pressure increases, both the friction coefficient and the rolling-sliding ratio increase. Whereas, when the sliding velocity changes, friction coefficient and rolling-sliding ratio change in opposite direction.

3.1.1. Velocity

In general, velocity at the contact point in a tripod type CV joint is related to the PCR. Even if the radius of the spherical roller changes, the actual travel distance of the center of the roller is the same in the articulated condition. Therefore, the design parameters related to the radius of the spherical roller are not considered.

TABLE 3.1 Change of design parameter

Value	Existing parameter	Changed parameter
PCR (mm)	22.75	18.2, 27.3
Contact angle (deg)	10	8, 12

Track curvature (mm)	44.2	35.36, 39.78, 48.62, 53.04

In this study, the design parameters were changed by ± 20% compared to existing design parameters, and the change of the velocity was analyzed according to the change of the design parameters. The changeable design parameters are shown in TABLE 3.1. In this chapter, PCR will be changed. Contact angle and PCR are related to the normal pressure.

As shown in Figure 3.1, in all torque range, the velocity decreases as the PCR increases and the velocity increases as the PCR decreases in all range of driving angular velocity. However, additional analysis is meaningless because PCR is related to size of the CV joint. This is because the vehicle type changes when the constant-velocity joint size changes and then the conditions under which the constant velocity joint is driven vary.

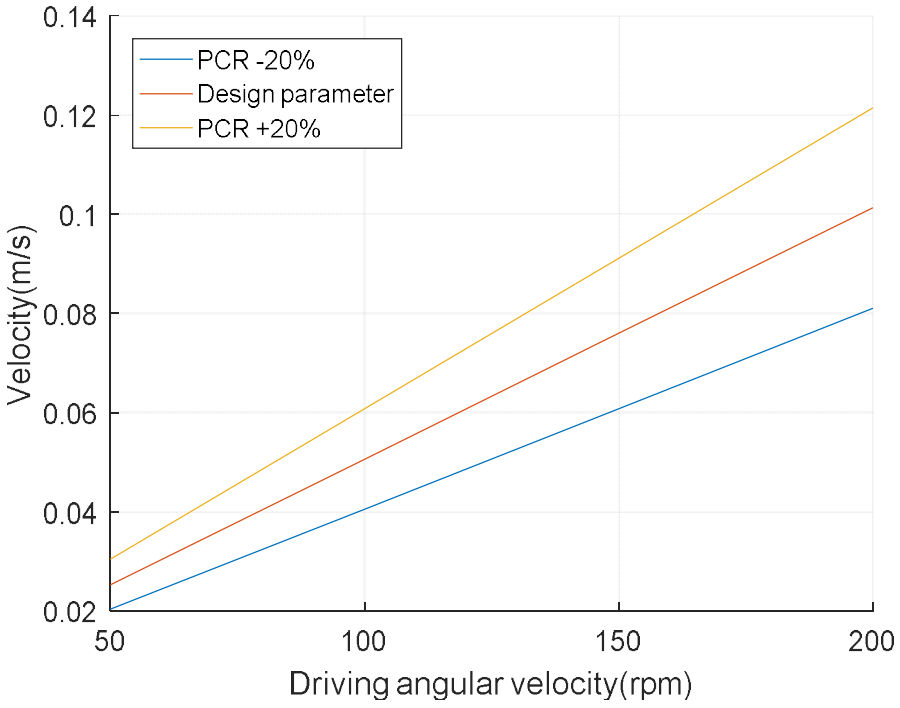

Figure 3.1 Change of velocity according to change of PCR

3.1.2. Normal pressure

At the contact point inside the constant velocity joint, the normal pressure is determined by the driving conditions and the geometrical characteristics. As mentioned above, since the driving condition is not a variable that can be changed,

the analysis of the normal pressure was carried out through geometrical characterization. Hertz's law was used to analyze geometric changes.

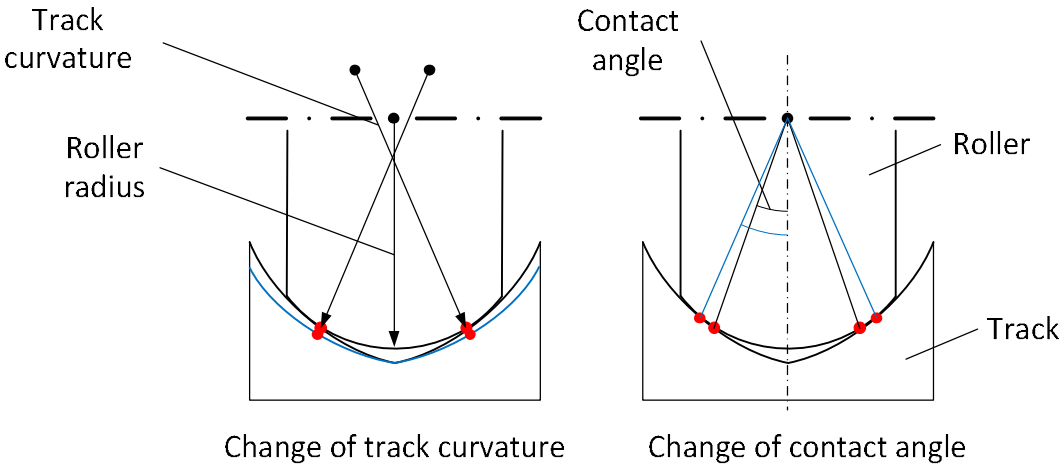

Figure 3.2 Design parameters related to normal pressure

The relationship between the normal pressure and the design parameters is shown in Figure 3.3. Because the sensitivity of the track curvature to the normal pressure is higher than that of the contact angle, the change of the track curvature is further divided into ± 10% as shown in TABLE 3.1.

The constraint ranges of the design parameters are shown in TABLE 3.2. The maximum value of the track curvature is infinity, that is, a straight line. The minimum value is equal to the radius of the spherical roller, and this value is about -26% of that of the original design parameters.

The maximum value of the contact angle is the angle at which the track and the roller end contact, which is about 19 degrees. The minimum value is 0 degree. In this case, the two-point contact is changed to one-point contact.

TABLE 3.2 Constraint ranges of design parameter

Value	Max	Min
Contact angle (deg)	18.85	0 (1 point contact)
Track curvature (mm)	∞	16.25

As shown in the Figure 3.3 (a), when the track curvature decreases, the normal pressure decreases. In the case of the contact angle as shown in Figure 3.3 (b), the normal pressure decreases as the contact angle increases.

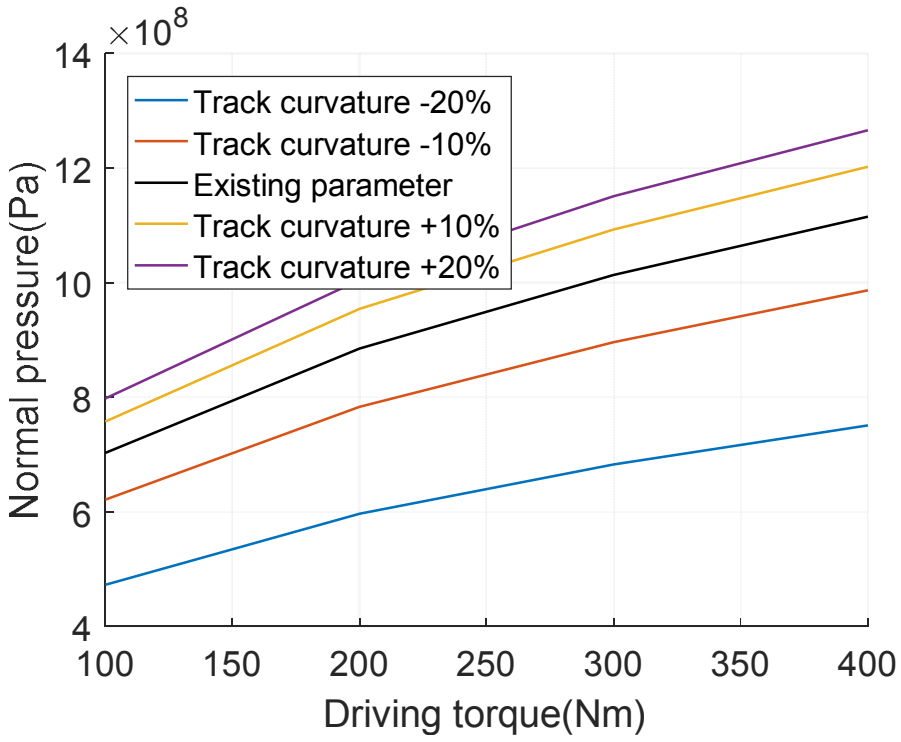

(a)

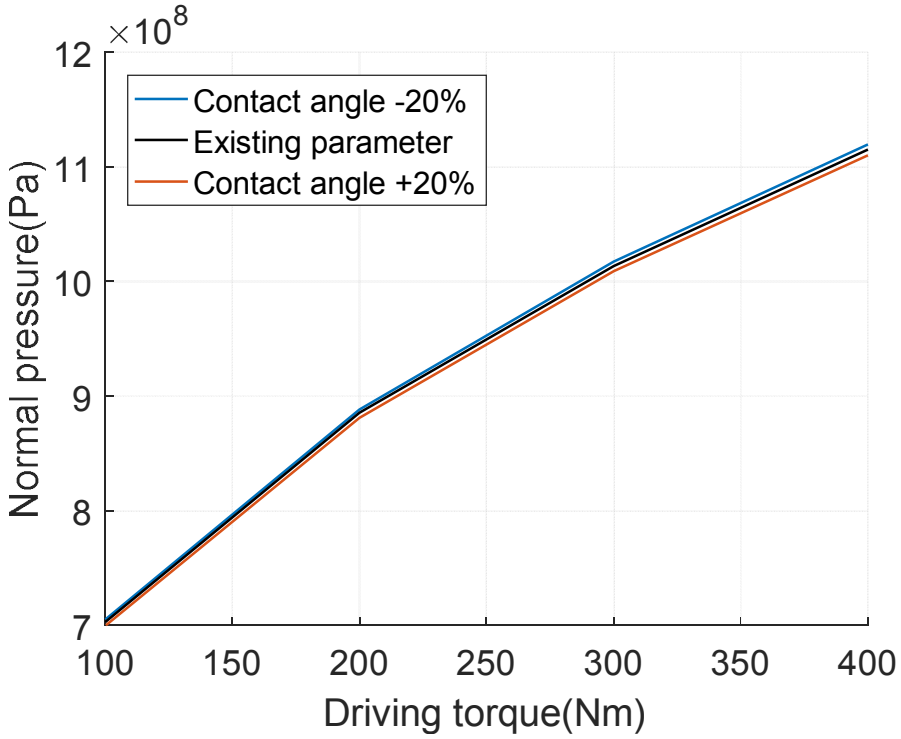

(b)

Figure 3.3 Change of normal pressure according to change of (a) track curvature and (b) contact angle

Analysis on the variation of the normal pressure according to the change of the track curvature and the contact angle was performed. Sensitivity analysis for each design parameter was conducted to compare the influence of each design

parameter on normal pressure more clearly. The analysis was carried out at 400 Nm, 200 rpm driving conditions. The results are shown in Figure. 3.4.

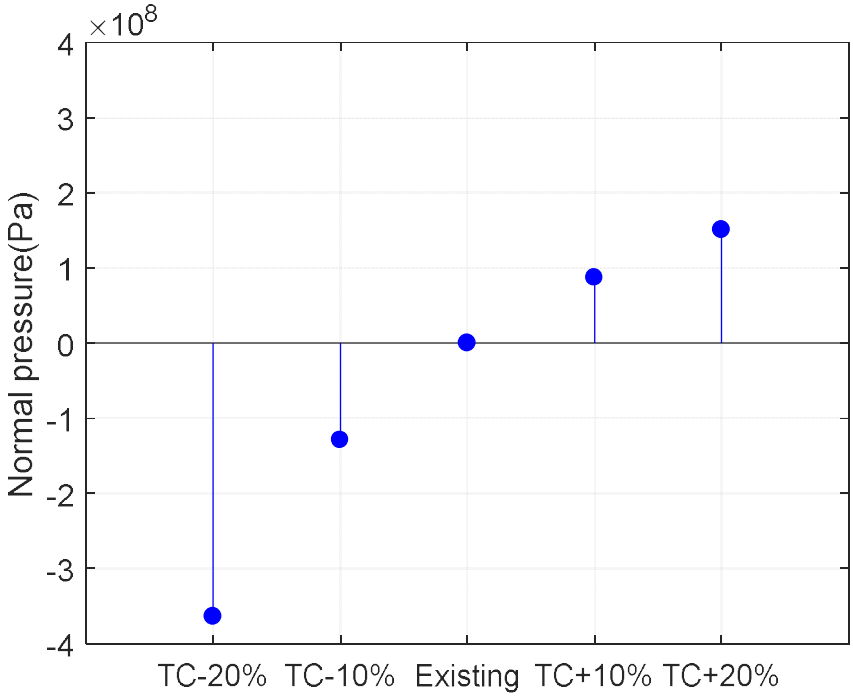

(a)

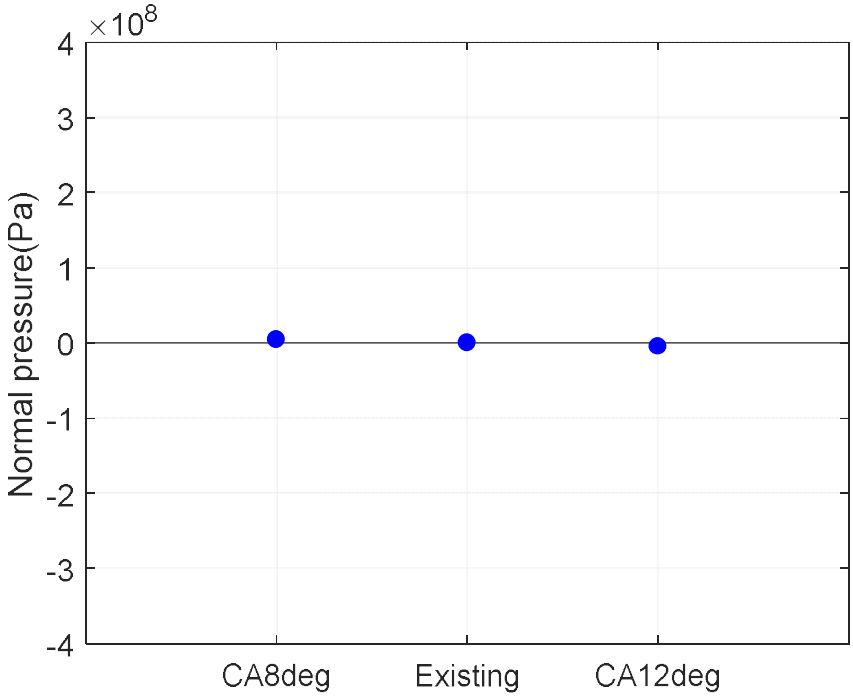

(b)

Figure 3.4 Design parameter sensitivity analysis on normal pressure of (a) track curvature (b) contact angle

As shown in Figure 3.4, the track curvature has more influence on normal pressure than the contact angle.

Based on the results, the optimized design parameter can be found. It is the combination of -20% track curvature and +20% contact angle. As shown in Figure 3.4, the normal pressure of the optimized design parameter is the lowest in all driving conditions. It means that GAF of optimized design parameter will be the lowest in all driving conditions.

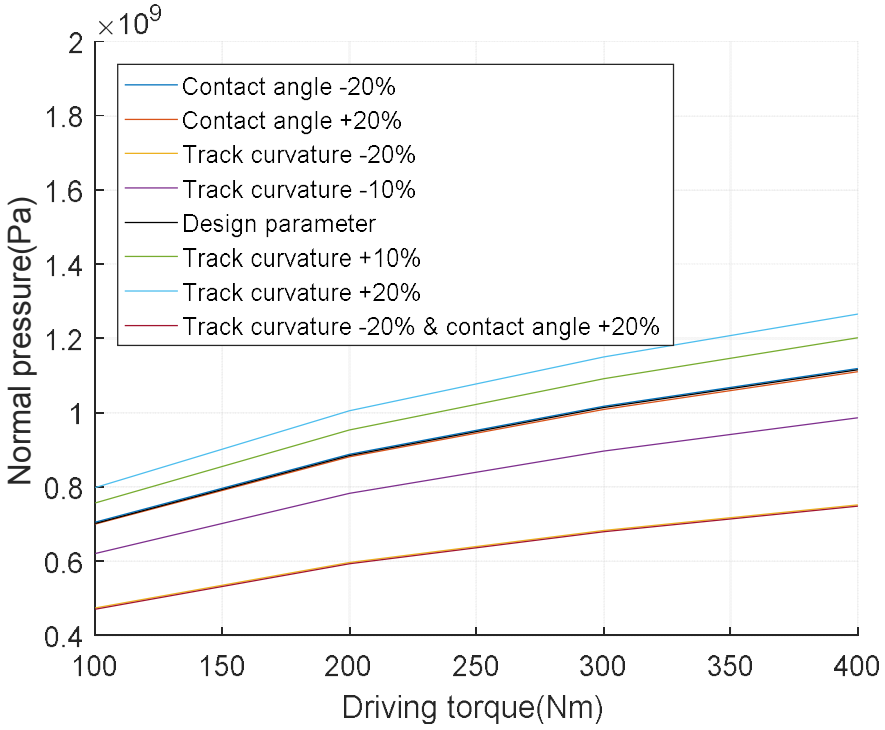

Figure 3.5 change of normal pressure according to design parameters

3.2. GAF estimation with changed design parameter

In the previous chapter, the GAF factors were analyzed to find out the relationship between the factors and the GAF. Through the developed GAF model, GAF estimation were carried out according to the change of the design parameters

which are related to the GAF.

GAF was estimated according to the change of the design parameters. Figure 3.6 shows GAF at 200 rpm with respect to resistance torque. Regardless of the design parameters, GAF increase with the increase of torque. In addition to its increase trend, the smaller the track curvature is, the higher GAF is and the larger the contact angle is, the higher GAF is. At 100 Nm, GAF changes from 8.34 to 8.42 N according to the change of contact angle and GAF changes from 7.99 to 8.59 N according to the change of track curvature. At 400 Nm, GAF changes from 37.13 to 37.49 N according to the change of contact angle and GAF changes from 33.96 to 37.63 N according to the change of track curvature. Difference in GAF increases as the torque increases. In all conditions, the change of GAF according to the change of the track curvature is larger than the change of GAF according to the change of the contact angle.

GAF of optimized design parameter has the lowest value in all conditions. In

the torque range from 0 to 400 Nm, GAF is in the range from 0 to 33.77 N. At 400 Nm, the GAF of optimized design parameter is 9.54 % smaller than that of existing design parameter.

The overall trend of GAF is similar to that predicted through factor analysis.

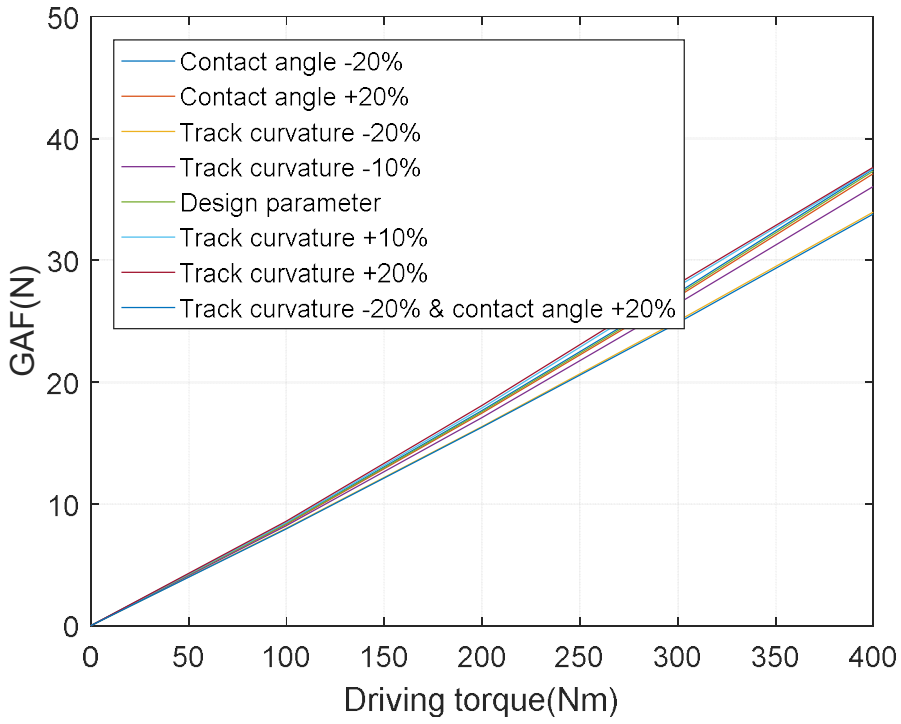

Figure 3.6 GAF estimation according to change of design parameters

Sensitivity analysis on GAF for each design parameter was conducted to compare the influence of each design parameter on GAF more clearly. The analysis was carried out at 400 Nm, 200 rpm driving conditions. The results are shown in Figure. 3.7.

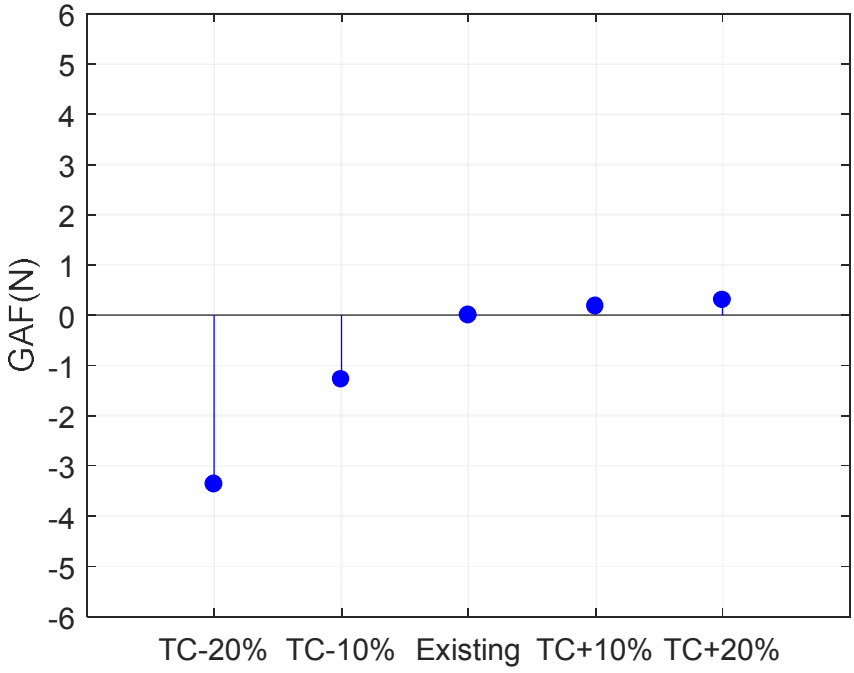

(a)

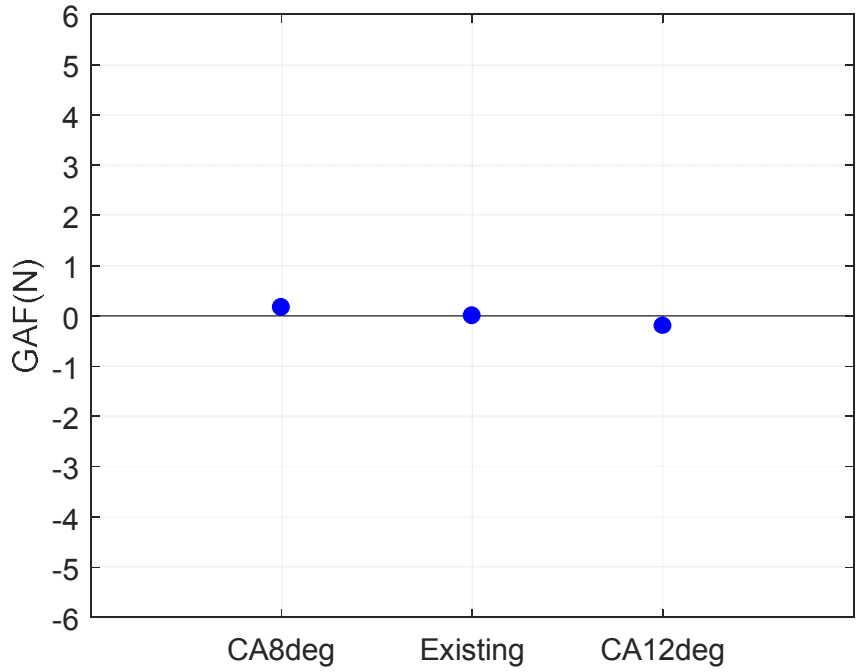

(b)

Figure 3.7 Design parameter sensitivity analysis on GAF (a) track curvature

(b) contact angle

As shown in Figure 3.7, the GAF decreases with the decrease of the track curvature and the GAF decreases with the increase of the contact angle.

3.3. Verification and GAF reduction

In the previous chapters, a GAF estimation model was developed through the kinematic analysis, normal pressure derivation and integrated friction characteristics. By using the GAF estimation model, GAF factor analysis was performed. Through the factor analysis, GAF was estimated with respect to the changed design parameters to suggest direction of GAF reduction.

In this chapter, a new GAF measurement system was set up to verify the GAF predicted above and the proposed direction of GAF reduction was also verified.

3.3.1. Experimental setup

In order to verify the estimated GAF according to the change of the design parameters, a new GAF measurement system was set up. As shown in Figure 3.8, the GAF measurement system consists of a servo motor, weights, two load cell, spherical roller pair and track. The servo motor applies the speed corresponding to

each condition, and the load cells attached to both ends of the track measures the frictional force generated by the spherical roller and the track, that is, the GAF.

Since this system directly measures one pair of a spherical roller and a track unlike the measurement system of Figure 2.19. Each driving torque conditions is converted into normal force conditions which is calculated through the developed GAF estimation model and it is applied on the spherical roller and the track. The experimental conditions are shown in TABLE 3.3.

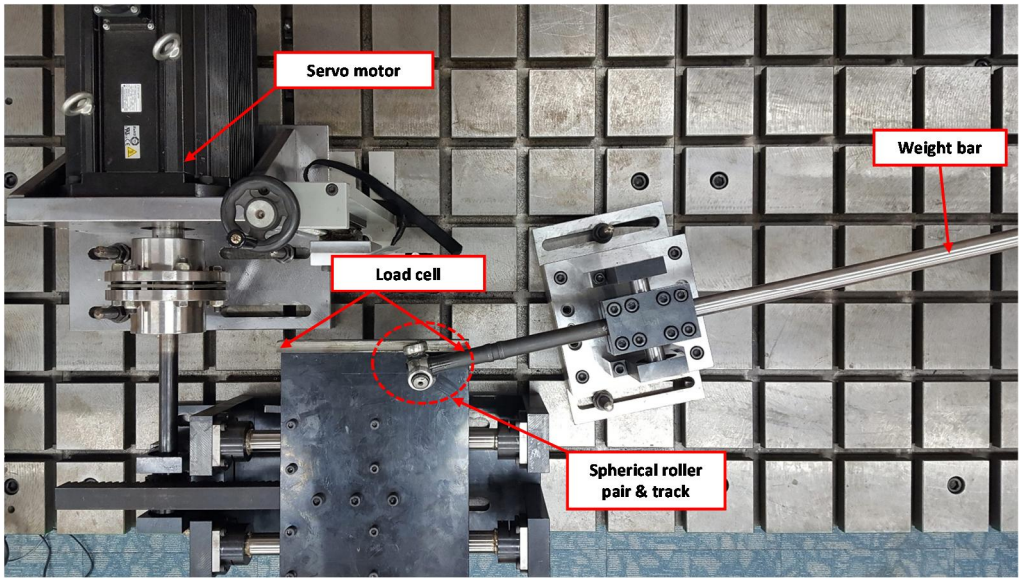

(a)

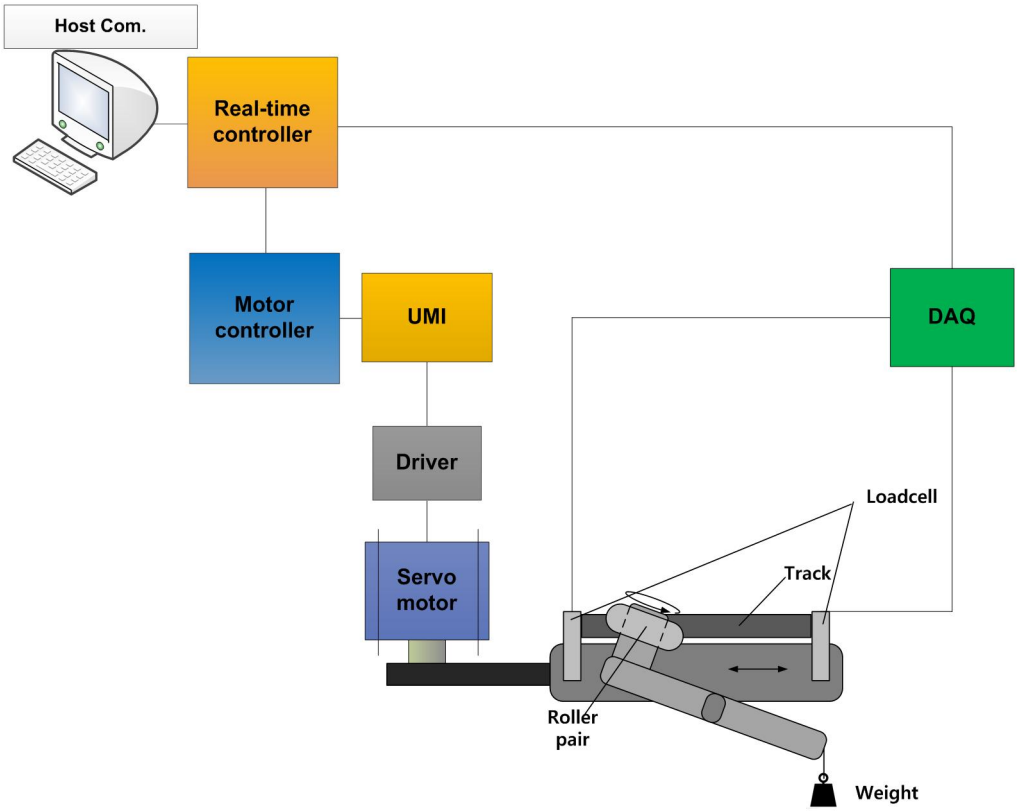

(b)

Figure 3.8 Experimental setup for GAF (1 roller) measurement: (a) the actual measurement system and (b) schematic diagram of the system

TABLE 3.3 GAF measurement conditions

Normal load (N)	773, 1546, 2319, 3092, 3864
Velocity (m/s)	0.01, 0.035, 0.06, 0.085, 0.11
Articulation angle (deg)	12

3.3.2. Verification and GAF reduction

For verification, GAF was measured through the GAF measurement system. Since the measured value was measured under normal force condition, it was converted to torque condition of 400 Nm as shown in TABLE 3.4, which is an actual driving condition, and it was compared with estimated value. First, the change of GAF according to the change of the contact angle was verified. As shown in Figure 3.9, the trend of the measured results is similar to the estimated results. As the contact angle increases, GAF decreases. The variation of the GAF according to the change of the contact angle is from 36.51 to 38.16 N. As

mentioned earlier, the change of the estimated GAF is from 37.13 to 37.49 N. It can be concluded that the GAF estimation model according to the change of the contact angle is verified by comparing the results.

TABLE 3.4 Verification conditions

Torque (Nm)	400
rpm (rpm)	200
Articulation angle (deg)	12

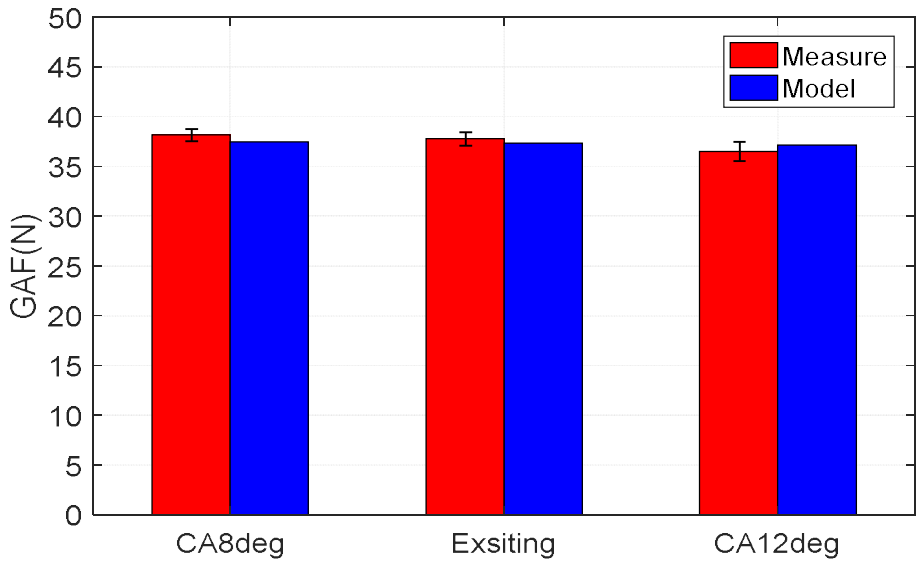

Figure 3.9 Verification according to change of contact angle

In the next, model is verified according to the change of the track curvature. As mentioned earlier, the influence of the track curvature on the normal pressure is larger than that of the contact angle, so the value of the track curvature is further subdivided into ±10 %. As shown in Figure 3.10, the trend of the measured results is similar to the estimated results. As the track curvature increases, the GAF increases. The variation of the GAF according to the change of the track

curvature is from 34.55 to 39.56 N. As mentioned earlier, the change of the estimated GAF is from 33.96 to 37.63 N. It can be concluded that the GAF estimation model according to the change of the track curvature is verified by comparing the results.

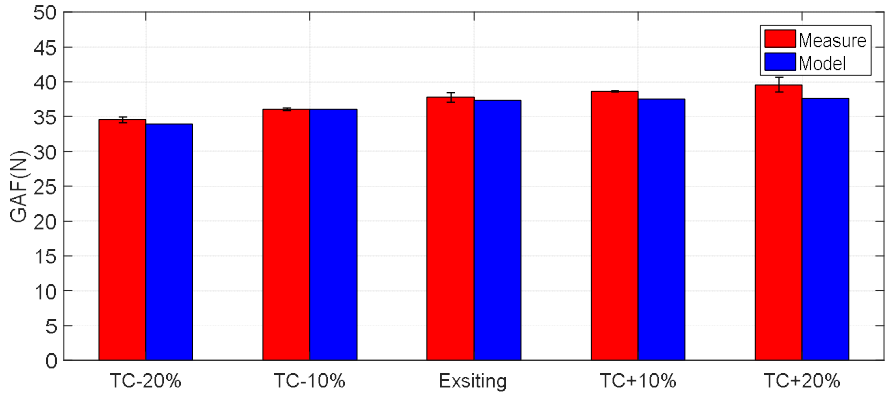

Figure 3.10 Verification according to change of track curvature

The final goal in this study is the reduction of GAF. In the previous chapter, optimized design variables for GAF reduction were selected, and the product was

fabricated to measure the GAF. As shown in Figure 3.11, it can be confirmed that the estimated value is similar to the measured value. The GAF of the optimized design parameter is 34.04 N and that of the existing design parameter is 37.76 N. GAF reduction is 3.72 N and that is 9.85 % of the GAF of existing design parameter. As a result, GAF reduction is verified.

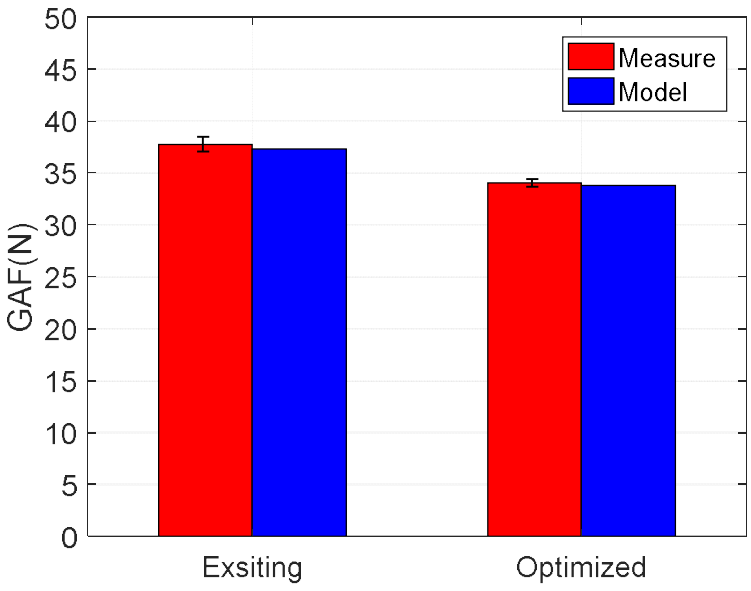

Figure 3.11 Verification of optimized design parameter

Chapter 4

4. Conclusion

In this study, a new GAF model considering two friction characteristics – pure sliding characteristics and rolling-sliding characteristics – was developed. By using the developed model, GAF factor analysis was performed and the direction for the reduction of the GAF was suggested and verified. As a final outcome, GAF reduction was achieved.

Firstly, for the development of the GAF model, relative motions were researched through kinematic analysis and the results were shown geometrically. The results included the relative movement of each component and the location of contact points.

Secondly, two friction characteristics which integrate pure sliding

characteristics with rolling-sliding characteristics were developed. In the pure-sliding friction characteristic, the factors of friction coefficient were analyzed by Hertz's law and geometrical approaches. In addition, the friction coefficients under various driving conditions were studied using a tribometer. From the analyzed results, the following results were obtained.

i) Friction coefficient increases with the increase of normal pressure.

ii) Friction coefficient increases with the decrease of sliding velocity.

iii) Friction coefficient increases with the increase of temperature.

In the rolling-sliding friction characteristic, rolling-sliding ratio was considered. The friction coefficient of rolling-sliding motion is the product of rolling-sliding ratio and sliding friction coefficient. In this study, in order for accurate GAF estimation, rolling-sliding ratio was experimentally studied and the results were used to obtain the friction coefficient of rolling-sliding motion. From the experimental studies on rolling-sliding ratio, this study can obtain the following

results.

i) Rolling-sliding ratio increases with the increase of normal pressure.

ii) Rolling-sliding ratio slightly increases with the increase of translation velocity.

By integrating two friction models into the geometrical analysis, a new GAF model was developed. In order to validate the GAF model, this study set a target tripod type CV joint and its GAF was estimated by the developed GAF model. From the estimation results, the following results were obtained.

i) GAF increases with the increase of articulation angle.

ii) GAF slightly increases with the decrease of rotation speed.

iii) GAF increases with the increase of resistance torque.

As the final procedure of development of GAF model, the GAF estimation results were experimentally verified. A GAF measurement system was set up and the GAF of the target CV joint were measured under the same driving condition

as the simulation. The measured GAF have similar tendency with the simulated results at low resistance torque and furthermore, the GAF model provides very accurate estimation at high resistance torque conditions such as 300 and 400 Nm.

In the next step of this study, sensitivity analysis of design parameters was performed by using the developed GAF model. The influence of the GAF factors were analyzed and main parameters were selected. New prototypes which have changed design parameters were manufactured and GAF of that was measured. Through the comparison the measured results with the estimated results, the results of the factor analysis were verified. Based on the results, the following results were obtained.

i) GAF increases with the increase of track curvature.

ii) GAF slightly increases with the decrease of contact angle.

Based on the results of factor analysis, the optimized design parameters were selected and its GAF was verified. The optimized design parameters are the

combination of -20 % track curvature and +20 % contact angle. Finally, the GAF of the optimized design parameters is reduced 9.85 % from the GAF of existing design parameters.

This study contributes to two aspects. It can be solution for existing method. First, relative motion. In this study, rolling-sliding ratio was consider, so accurate relative motion can be predicted.

Next, the actual friction coefficients and the rolling-sliding ratio were measured, so the change of design parameter can be reflected. It means that the direction for GAF reduction can be suggested. In addition, since the GAF can be predicted through the model developed in this study, the results of this study can be usefully used in the constant velocity joint design stage.

In this study, the detailed friction characteristics were considered. Thus, it is also used for analyzing idle booming and efficiency loss which are generated by the internal friction.

References

1. *Wagner, E. and C. Cooney, Universal joint and driveshaft design manual. Society of Automotive Engineers, Warrendale, PA, 1979: p. 127-129.*
2. *Schmelz, F., H.C. Seherr-Thoss, and E. Aucktor, Universal Joints and Driveshafts. 1991: Springer-Verlag.*
3. *Watanabe, K., T. Kawakatsu, and S. Nakao, Kinematic and static analyses of tripod constant velocity joints of the spherical end spider type. Journal of Mechanical Design, 2005. 127(6): p. 1137-1144.*
4. *Lim, Y.H., et al., Multibody dynamics analysis of the driveshaft coupling of the ball and tripod types of constant velocity joints. Multibody System Dynamics, 2009. 22(2): p. 145-162.*
5. *Serveto, S., J.P. Mariot, and M. Diaby, Modelling and measuring the axial force generated by tripod joint of automotive drive-shaft. Multibody System Dynamics, 2007. 19(3): p. 209-226.*
6. *Serveto, S., J.P. Mariot, and M. Diaby, Secondary torque in automotive drive shaft ball joints: influence of geometry and friction. Proceedings of the Institution of Mechanical Engineers Part K-Journal of Multi-Body Dynamics, 2008. 222(3): p. 215-*

227.

7. *Lee, C.H. and A.A. Polycarpou, A phenomenological friction model of tripod constant velocity (CV) joints. Tribology International, 2010. 43(4): p. 844-858.*
8. *Urbinati, F. and E. Pennestrì, Kinematic and dynamic analyses of the tripode joint. Multibody System Dynamics, 1998. 2(4): p. 355-367.*
9. *Mariot, J.P. and J.Y. K'Nevez, Kinematics of tripode transmissions. A new approach. Multibody System Dynamics, 1999. 3(1): p. 85-105.*
10. *K'nevez, J., et al., Kinematics of transmissions consisting of an outboard ball joint and an inboard generalized tripod joint. Proceedings of the Institution of Mechanical Engineers, Part K: Journal of Multi-body Dynamics, 2001. 215(3): p. 119-132.*
11. *Mariot, J.P., J.Y. K'Nevez, and B. Barbedette, Tripod and ball joint automotive transmission kinetostatic model including friction. Multibody System Dynamics, 2004. 11(2): p. 127-145.*
12. *Mariot, J. and J. K'nevez, Dynamics of an automotive transmission consisting of a tripod joint and a ball joint. A symbolic approach. Proceedings of the Institution of Mechanical Engineers, Part K: Journal of Multi-body Dynamics, 2002. 216(3): p. 203-211.*
13. *Wang, X.F., D.G. Chang, and J.Z. Wang, Kinematic investigation of tripod sliding universal joints based on coordinate transformation. Multibody System Dynamics,*

2009. 22(1): p. 97-113.

14. *Chang, D.G., et al., Lubricating Properties of Tripod Sliding Universal Joints Considering Thermal Effect. Tribology Transactions, 2010. 53(4): p. 502-510.*
15. *Wang, X.F. and D.G. Chang, Numerical Analysis on Lubricating Properties of Tripod Sliding Universal Joints. Tribology Transactions, 2008. 52(1): p. 86-95.*
16. *Kimata, K., et al., Numerical Analyses and Experiments on the Characteristics of Ball-Type Constant-Velocity Joints. JSME International Journal Series C, 2004. 47: p. 746-754.*
17. *Hamrock, B.J., Ball bearing lubrication : the elastohydrodynamics of elliptical contacts / Bernard J. Hamrock, Duncan Dowson, ed. D. Dowson. 1981, New York: New York : Wiley, c1981.*
18. *Popov, V.L., Contact Mechanics and Friction. 2010, Dordrecht: Dordreht : Springer.*
19. *Bhushan, B., Introduction to Tribology. 2013: Wiley.*
20. *Kalker, J.J., Three-Dimensional Elastic Bodies in Rolling Contact. Vol. 2. 1990: Springer Science & Business Media.*
21. *Johnson, K.L., Contact Mechanics. 1985: Cambrige.*
22. *Johnson, K., J. Greenwood, and S. Poon, A simple theory of asperity contact in elastohydro-dynamic lubrication. Wear, 1972. 19(1): p. 91-108.*
23. *Ludema, K.C., Friction, Wear, Lubrication. 1996: CRC.*
24. *Bhushan, B., Principles and Applications to Tribology. 2013: Wiley.*

25. *Yamaguchi, Y., F. Kennedy, and T. Blanchet, Tribology of Plastic Materials. 1991: American Society of Mechanical Engineers.*

26. *Mizuno, T. and M. Okamoto, Effects of Lubricant Viscosity at Pressure and Sliding Velocity on Lubricating Conditions in the Compression-Friction Test on Sheet Metals. Journal of Lubrication Technology-Transactions of the Asme, 1982. 104(1): p. 53-59.*

국문 초록

본 논문에서는 차량의 셔더 현상을 일으키는 트라이포드 타입 등속조인트의 축력을 예측하기 위한 모델링 방법을 제안하였다. 모델 개발을 위해, 기구학적 분석을 수행하여 각 부품들의 상대좌표 및 접촉점 좌표를 도출하였고, 그 결과를 기반으로 구동 조건으로부터 각 접촉점의 수직력을 계산하였다. 본 논문에서는 신뢰성 있는 축력 예측 모델 개발을 위해 상세 마찰 특성을 분석하였다. 이를 위해, 순수 슬라이딩 마찰 특성과 롤링-슬라이딩 마찰 특성을 이론 및 실험적인 상세한 분석을 통합하여 모델링에 적용하였다. 순수 마찰 특성의 마찰 계수는 실제 등속조인트 구동 조건으로부터 계산한 마찰 측정 조건을 바탕으로 트라이보미터를 이용해 실측하였다. 롤링-슬라이딩 마찰 특성의 마찰 계수는 순수 마찰 계수와 롤링-슬라이딩 비율의 곱으로 이루어져있기 때문에 롤링-슬라이딩 비율에 대한 분석을 진행하였다. 복합적인 마찰 특성을 분석하여 이를 모델링에 적용함으로써 신뢰성 있는 축력 예측 모델링을 완성하였다.

본 연구에서는 축력 예측 모델 검증을 위해 축력 측정 시스템을 구축하였다. 각 구동 조건에서 축력 측정값과 축력 예측 모델링을 통해 예측한 축력 값 비교를 통하여 축력 예측 모델링을 검증하였다. 예측한 축력 값은 절각 조건 및 토크 조건, 각속도 조건에 변화에 따라 측정값과 비교 하였고 그 결과, 측정값과 거의 일치하는 경향성을 보이는 것을 확인하였다. 또한, 각 조건에서의 비교를 통해 정확한 예측 값을 갖는 것을 확인하였다.

본 연구에서는 개발된 축력 예측 모델을 이용하여 축력 관련 인자 분석을 진행하였다. 각 인자들의 축력에 대한 민감도를 분석하고, 분석 결과를 바탕으로 축력 관련 주요 인자를 선정하였으며 실제 인자들의 변경 값을 적용한 제품을 제작하여 축력 측정 시스템을 통해 축력을 측정하였다. 측정한 값과 개발된 모델에 변경된 설계 인자를 적용하여 예측한 축력 값과의 비교를 통해 설계 인자 변경에 따른 축력 민감도 분석을 검증하였다. 최종적으로 앞 선 결과를 바탕으로 축력 저감을 위한 최적의 설계 인자를 선정하여 이를 제작하였고, 축력 측정을 통해

축력이 감소된 것을 확인하였다.

주요어: 축력, 등속조인트, 트라이포드 타입 등속조인트, 수직력, 상대 좌표, 마찰 특성, 마찰 계수, 롤링-슬라이딩 비율, 스페리컬 롤러, 트랙, 트랙 곡률, 접촉각, 수직 압력, 속도, 축력 저감

학번: 2010-23233